Paleoseismic evidence of clustered earthquakes on the San Andreas fault in the Carrizo Plain, California

Lisa B. Grant[1] and Kerry Sieh

Seismological Laboratory, California Institute of Technology, Pasadena

Abstract. Exposures we have excavated across the San Andreas fault contradict the hypothesis that part of the fault in the Carrizo Plain is unusually strong and experiences relatively infrequent rupture. The exposures record evidence of at least seven surface-rupturing earthquakes which have been approximately dated by accelerated mass spectrometry radiocarbon analysis of detrital charcoal and buried in situ plants. Five large earthquakes have occurred since 1218 A.D. The most recent earthquake, event A, was the 1857 Fort Tejon earthquake, which we have associated with 6.6–10 m of dextral slip along the main fault trace. The penultimate earthquake, event B, most likely occurred within the period A.D. 1405–1510. Slip from either events B and C combined or from event B alone, totals 7–11 m. Three earthquakes, events C, D, and E, occurred in a temporal cluster prior to event B and after approximately A.D. 1218. The average recurrence interval within this cluster is 73–116 years, depending on assumptions. Events F and G occurred after 200 years B.C. A depositional hiatus between events E and F may hide evidence of additional earthquakes. Events B and D within the Carrizo cluster of A.D. 1218–1510 may correlate with events T (A.D. 1329–1363) and V (A.D. 1465–1495) at Pallett Creek on the Mojave "segment" of the fault. This suggests two fault ruptures similar in length to that of 1857. Events C and E apparently did not rupture the Mojave section, which suggests that the Carrizo segment has ruptured independently or in combination with segments to the north. Irregular repeat times of large earthquakes suggest a pattern of clustered events at the end of seismic "supercycles."

Introduction

Within the past two decades, geologists and seismologists looking at ancient and modern patterns of large earthquakes have concluded that active faults typically do not generate regular patterns of earthquake recurrence [*Sieh et al.*, 1989; *Jacoby et al.*, 1988; *Thatcher*, 1989; *Matsuda et al.*, 1978]. These discoveries have inspired theoretical work that suggests that even deterministic physical systems may produce complex temporal and spatial patterns of fault rupture [*Rundle*, 1988; *Stuart*, 1986; *Ward*, 1992]. The timing and rupture extent of large earthquakes may even be chaotic, rather than time-predictable or characteristic [*Huang and Turcotte*, 1990; *Scholz*, 1990].

Nevertheless, several observations and models suggest that the strongest segments of faults may control the timing of the largest earthquakes along a fault and may have histories that most closely approximate uniform recurrence [*Thatcher*, 1989; *Sieh et al.*, 1989; *Ward*, 1992]. In this paper we report data that enable a test of this idea.

The Carrizo segment of the San Andreas fault (Figure 1) has been interpreted as an unusually strong fault segment [*Sieh and Jahns*, 1984; *Schwartz and Coppersmith*, 1984; *Sykes and Seeber*, 1985; *Stuart*, 1986] which ruptures relatively infrequently during large earthquakes. The basis for

this hypothesis is geomorphic. This segment experienced the largest offsets during the latest large earthquake, in 1857. Previous measurements of stream channels offset 9.5, 21.8, and 33 m near Wallace Creek (Figure 1) suggest that 9.5, 12.3, and 11 m of dextral slip occurred during the past three large earthquakes. If strain accumulates uniformly at the average Holocene slip rate of 34 ± 3 mm/yr and if it is relieved according to a time-predictable model, then the time intervals following these three earthquakes should be 250–450 years [*Sieh and Jahns*, 1984].

Recent geomorphic and geodetic measurements, respectively, confirm that 6.6–10 m of dextral slip occurred on the main trace, and 11.0 ± 2.5 m (1σ) of displacement occurred across the San Andreas fault zone in the Carrizo Plain during the 1857 earthquake [*Grant and Sieh*, 1993; *Grant and Donnellan*, 1994]. Recent geologic work has confirmed that the previous large earthquake occurred several centuries prior to 1857 [*Grant and Sieh*, 1993]. More precise dates and offsets of this penultimate event, and its predecessors, have, until now, been unavailable. Without such data the above mentioned earthquake recurrence hypotheses are highly speculative.

Relatively complete paleoseismic records of earthquake dates spanning more than a few earthquake cycles have previously been available at only two sites along the Mojave segment: the Pallett Creek and Wrightwood sites (Figure 1) [*Sieh et al.*, 1989; *Fumal et al.*, 1993]. More complete sets of dates and slip in prehistoric earthquakes elsewhere along the fault are needed to formulate better models of fault behavior and seismic hazard. This paper presents and interprets

---

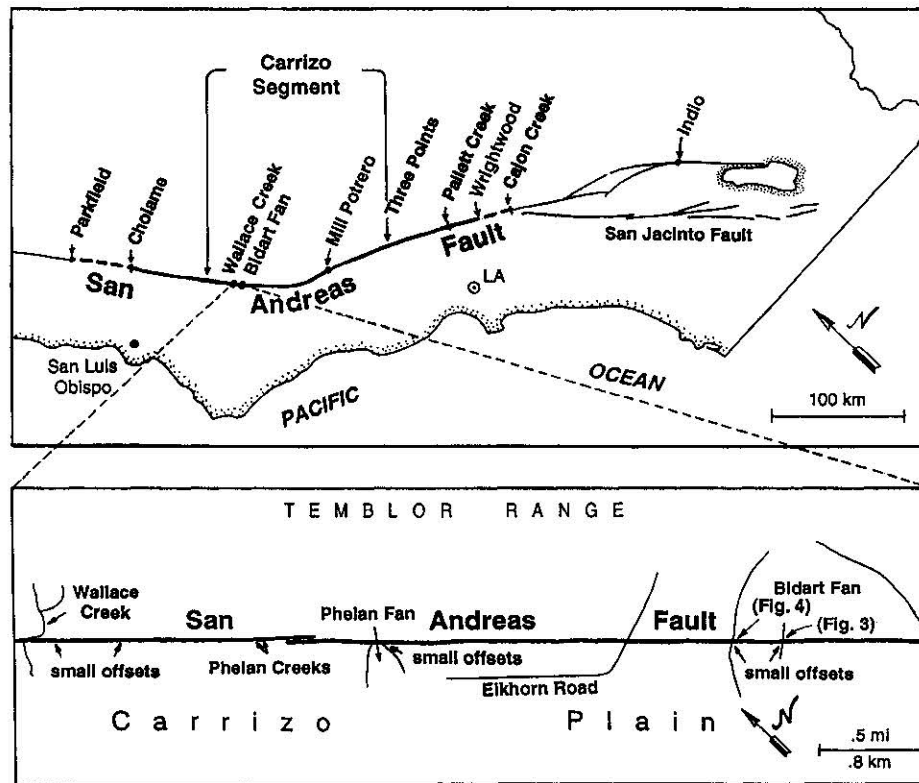[1]Now at Woodward-Clyde Consultants, Santa Ana, California.

Figure 1. Map of the southern San Andreas fault, with 1857 rupture in bold and dashed where uncertain. The study site is located on the Carrizo segment of the fault, the segment which contains the largest offsets associated with the great 1857 earthquake [*Sieh*, 1978; *WGCEP*, 1988]. Inset map shows local features mentioned in the text.

additional evidence of past large earthquakes on the Carrizo segment of the San Andreas fault.

Site Selection

To determine the dates and offsets associated with the past several large earthquakes, we sought a site where sediment has been accumulating across the fault over the past millenium. To allow discrimination of individual events, the sedimentation must have occurred more frequently than surface-rupturing earthquakes. For optimum use of radiocarbon dating methods, the time interval between depositional events should be less than the error bars on radiocarbon analyses, that is, less than a few decades.

In the semiarid Carrizo Plain, sediment is deposited primarily as debris flows on alluvial fans during the wetter winter months. Inspection of twentieth-century aerial photos indicates that storm runoff deposits sediments on the fans every decade or two. However, the locus of deposition migrates across the fans on a timescale that is much longer than the interval between storms. Therefore areas on the fans experience long hiatuses in deposition interspersed with periods of frequent sedimentation. Hence for this study we sought an aggrading alluvial fan, traversed by the San Andreas fault and with a discernible pattern of prehistoric sedimentation. On the Bidart Ranch 5–6 km southeast of Wallace Creek the fault traverses an alluvial fan that appeared on geomorphic grounds to meet this requirement.

Bidart Fan

The Bidart fan is fed by ephemeral streams that drain the western flank of the Temblor Range and the northern Panorama Hills (Figures 1 and 2). The fan is heavily grazed and sparsely vegetated. Photographs taken in 1966 and 1978
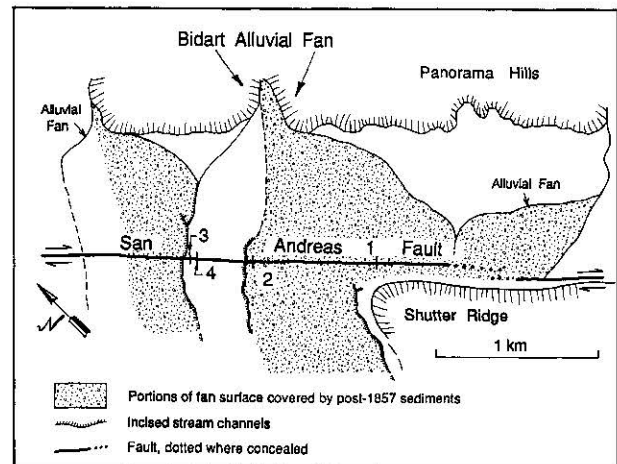

Figure 2. Map of the Bidart alluvial fan and nearby fans, showing locations of trenches, entrenched and offset stream channels. Stippled pattern marks recent deposition, mapped from 1966 and 1978 air photos and from ground inspection in 1991. Base: from 1:6000 and 1:35000-scale aerial photographs taken in 1966 and 1978.
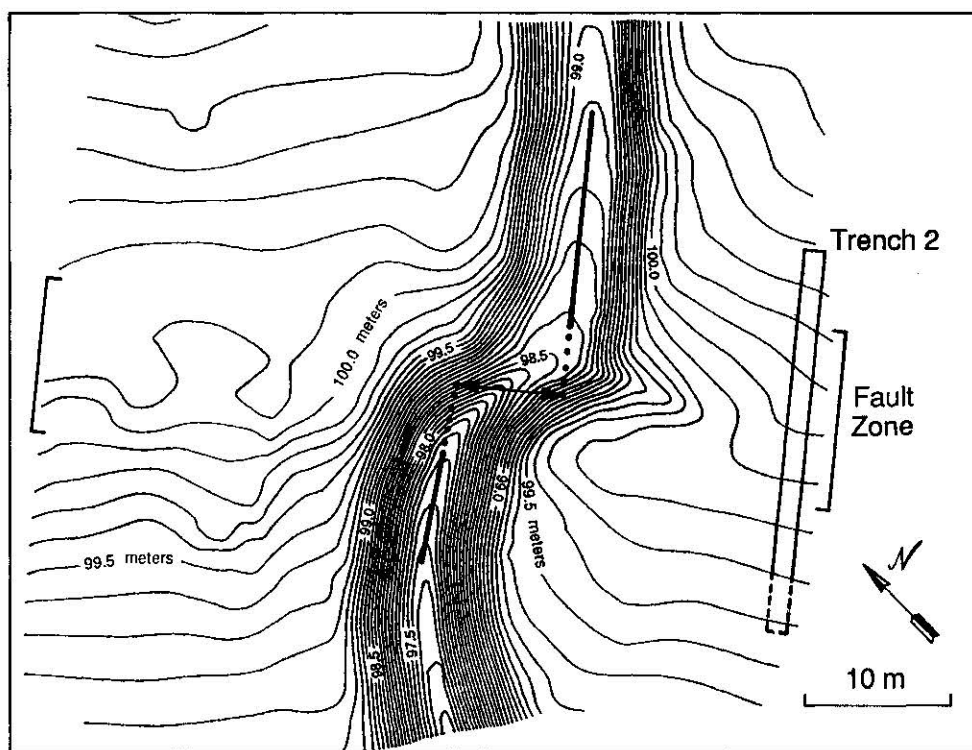
Figure 3. Topographic map of the offset stream channel near the middle of the Bidart alluvial fan. Contour interval is 10 cm, and elevations are measured relative to an arbitrary datum. The channel was cut and the fan surface northwest of the channel became inactive prior to A.D. 1857. The walls of trench 2 shown in Figure 5 are solid. Unmapped ends of the trench are dashed. The fault zone, as exposed in the trench, is indicated with brackets. The mismatch of thalwegs (thick solid lines) outside the fault zone indicates dextral offset of the channel. To measure the amount of offset, the thalwegs are projected to the middle of the fault zone. Different projections of the thalweg yield different offset measurements. The projection shown yields an offset measurement of 7 m. If the thalweg was a straight line across the fault prior to the 1857 earthquake, then the offset would be 8 m. If there is unrecognized warping outside the fault zone, then the amount of offset could be greater.

show recent sediments covering the southeastern part of the fan. Floods in 1991 buried an even larger area with fresh sediment, but negligible deposition occurred on the northwestern part of the fan.

The surficial pattern of sedimentation and channel incision on the Bidart fan suggests that the area of active sedimentation has swept across the fan from northwest to southeast over the time period of several earthquake cycles. Northwest of the center of the fan, near trench 2, an incised stream channel is offset by the fault (Figure 3). We suspected that this offset formed during the 1857 earthquake because the Phelan fan and a channel 3 km to the northwest (Figure 1) were offset approximately the same amount during the 1857 earthquake [*Grant and Sieh*, 1993]. Therefore the adjacent northwestern part of the Bidart fan had probably been actively sedimenting prior to but not since 1857. At the northwestern edge of the fan another incised ephemeral channel is offset 14.6–18.4 m (Figure 4). This larger amount of slip would represent at least the 1857 and one previous prehistoric earthquake. Thus parts of the fan adjacent to the larger offset probably were active before but not after the last two or more earthquakes.

From these geomorphic clues we anticipated we would be able to piece together a complete recurrence story from several well-placed excavations across the Bidart fan. Trench 1, excavated by *Prentice and Sieh* [1989] on the

southeastern lobe of the fan, revealed frequent sedimentation from about A.D. 1500 to the present. The 1857 earthquake was clearly expressed within the upper 1-m-thick section. Deeper in the section, three depositional hiatuses of several hundred to a thousand years duration led *Prentice and Sieh* [1989] to conclude that their record of seven earthquakes in 3000 years B.P. was a minimum. From this partial record they calculated a maximum average recurrence interval of 500 years.

Because the channel near trench 2 is offset roughly half as much as the channel near trenches 3 and 4, the channel near trench 2 must have incised sometime between 1857 and the penultimate earthquake. Therefore we expected to find a better record of the penultimate event near the smaller offset because we hypothesized that sediment was deposited on the central portion of the fan prior to incision of the channel. We placed trench 2 next to the smaller offset to search for evidence of the penultimate earthquake (Figure 3). Because the incised channel offset 14.6–18.4 m at the northwestern edge of the Bidart fan was presumably formed by more than one earthquake [*Sieh*, 1978], the northwestern part of the fan would have been the depositional lobe of the fan between the penultimate event and one or more previous events. Therefore we placed trench 3 next to this offset and trench 4 astride a small graben nearby to examine evidence of older earthquakes (Figure 4).
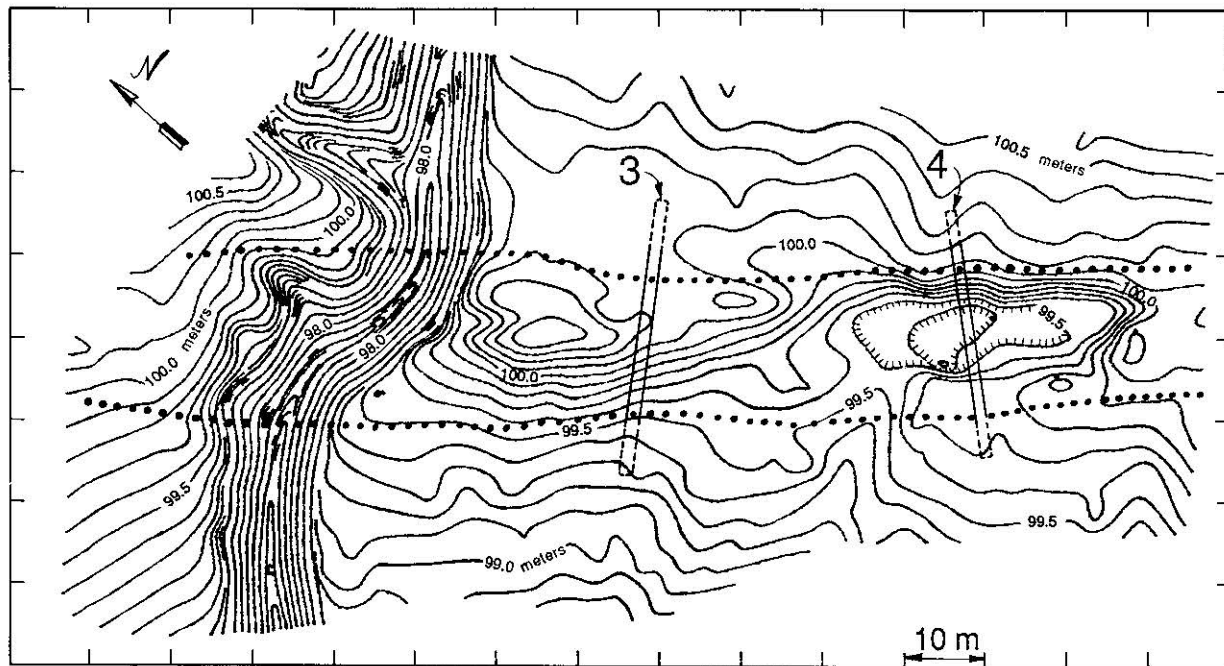
Figure 4. Topographic map of the fault zone in vicinity of trenches 3 and 4. Contour interval is 10 cm. Trench 3 cuts a moletrack, and trench 4 traverses a tectonic depression. The large (14.6–18.4 m) offset of the channel indicates that this northwestern margin of the Bidart alluvial fan was inactivated prior to at least A.D. 1857 and a prior large slip event. Structural and stratigraphic relations in the trenches constrain the date of abandonment of the surface (see text). The mapped portions of trenches 3 and 4, shown with solid lines, are displayed in cross section in Figures 8 and 9. Approximate width of the fault zone in recent surficial-rupture events is delimited with bold dots.

Methods

After excavating the trenches, we cleaned off, surveyed, and mapped the walls in detail at a scale of 1:20. We collected hundreds of samples of organic material and charcoal from the trench walls. Only a few of these samples were large enough for radiocarbon dating by accelerator mass spectrometry (AMS).

We recorded stratigraphic evidence of surficial rupture associated with earthquakes. Several stratigraphic features indicate large prehistoric earthquakes. Events are recognized in the trench walls primarily by broken and tilted beds overlain by unbroken beds and by upward terminations of fault traces. A single upward termination of a fault trace may be tenuous evidence for an event [*Bonilla and Lienkaemper*, 1990], especially if the vertical separation across the fault is less than a few centimeters. To be confident of a distinct event, evidence must exist at the same stratigraphic horizon at several locations in the trench and on both walls. Therefore all of the events we report were caused by substantial surficial rupture, probably of the order of a meter or more. Fault zone breccia is distinguished from bioturbated zones by vertical fabrics and facies changes or differences in beds on opposite sides of the zone. We assign letter names to each event and describe the evidence in each trench.

Trench 2 and the Penultimate Earthquake

Structure and Stratigraphy

Trench 2 was cut next to the smaller offset to search for subsurficial evidence of a large earthquake prior to the 1857

earthquake. Figure 5 is a simplified cross section of the faults and major units in the walls of a portion of trench 2. The stratigraphic position and lithologic description of the beds in this trench are summarized in Figure 6. The beds are numbered to facilitate discussion. Primary sedimentary structures are preserved in the upper half of the section above unit 20, except for bioturbated unit 1, immediately below the present ground surface. Most beds are hardened debris flows or loose fluvial deposits ranging in texture from finely laminated silts to gravels. Several beds thin to the southwest or pinch out against paleofault scarps (Figure 5). The sense of apparent displacement across several faults is down to the northeast, suggesting that northeast facing scarps may have ponded the thicker beds to the northeast.

Paleosols and Bioturbated Horizons

Long and short depositional hiatuses are represented by thick bioturbated layers and thin paleosols, respectively. We estimate the time required to form these paleosols and bioturbated zones from dated horizons in trench 1 [*Prentice and Sieh*, 1989; also written communication, 1993]. The paleosols are A_v horizons up to a few centimeters thick formed by small roots and the expansion of soil gases. They are characterized by vesicles and tubes up to a millimeter or two in diameter, sharp upper boundaries, and irregular lower limits that cut across laminations of subjacent beds. Field observations after the 1991 storms indicate that growth of grasses and other plants initiate paleosol development a few weeks to months after deposition of fine sediment. In trench 1 more than 70 cm of sediment has been deposited since
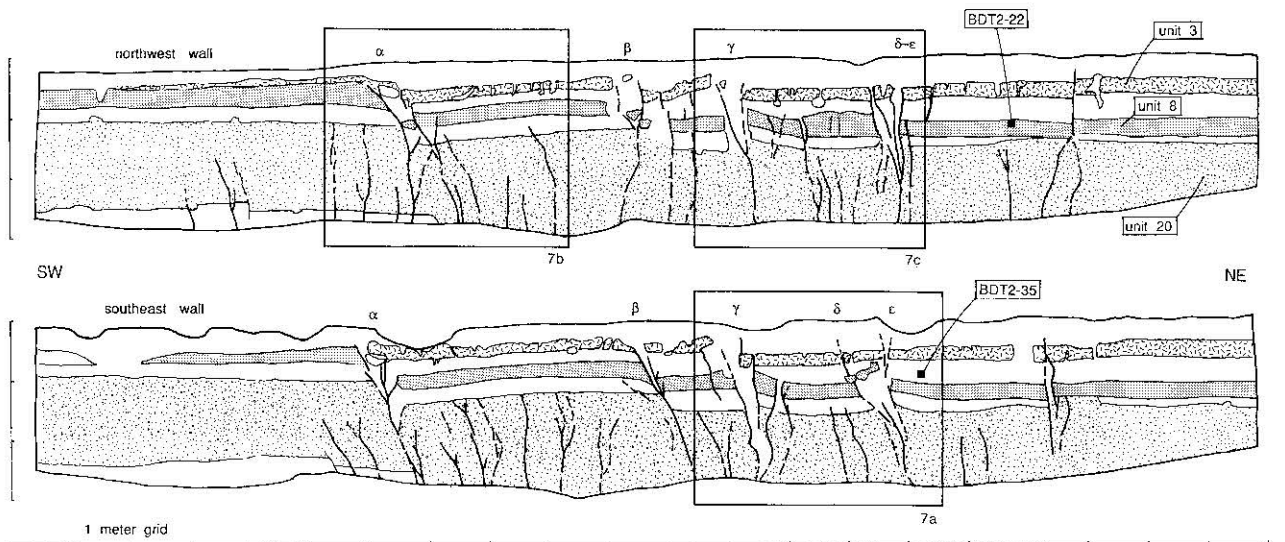
Figure 5. Cross section through sediments in the walls of trench 2 shows fault traces, radiocarbon sample locations, and units 3, 8, and 20. The ground surface ceased being an active fan surface prior to A.D. 1857, so the faults of the latest great earthquake extend to the ground surface. At least two prehistoric disruptions also appear in these trench walls. Boxes outline stratigraphic sections shown in detail in Figures 7a–7c, where stratigraphic levels of the three disruptions are especially clear. View is toward the northwest.

1857. Five thin paleosols occur in the sediments above the horizon of the last earthquake [*Prentice and Sieh*, 1989, also written communication, 1993]. Therefore six paleosols, each a centimeter or two thick, have formed since the last earthquake at the site of trench 1. The average period between these thin paleosols is therefore no more than about two decades.

Two bioturbated zones, each 40–100 cm thick, were also mapped in the exposures of trench 1 (C. S. Prentice and K. Sieh, written communication, 1993). These are characterized by unbedded, heterogeneous, silty, pebbly sand with sharp upper and very irregular lower boundaries. Circular filled tubes up to several centimeters in diameter and semicircular boundaries indicate that rodents have been the primary agents of disruption. The thickness of the bioturbated zones, relative to the paleosols, suggests that they formed during time periods when the rate of bioturbation exceeded the rate of sedimentation, that is, when the active lobe of the fan was depositing sediment elsewhere. Radiocarbon dates of beds in trench 1 above and below the bioturbated zones indicate that these depositional hiatuses lasted at least 250 but no more than 1000 years (C. S. Prentice and K. Sieh, written communication, 1993).

In trench 2 a bioturbated layer with scattered remnants of original sedimentary structure forms the lower half of the section above several debris flow beds at the base of the trench. This layer, unit 20, represents a hiatus in deposition when the active lobe of the Bidart fan was depositing sediment on another part of the fan. Three paleosols form time-stratigraphic markers across much of trench 2. A 1–4-cm-thick paleosol with root holes, high porosity, and random grain orientation is present in the matrix supporting the pebbles at the top of unit 9 (Figure 6). A poorly developed, discontinuous paleosol of similar appearance is present near the base of laminated silt and sand bed 8. It indicates that unit 8 was deposited by more than one sedimentary event.
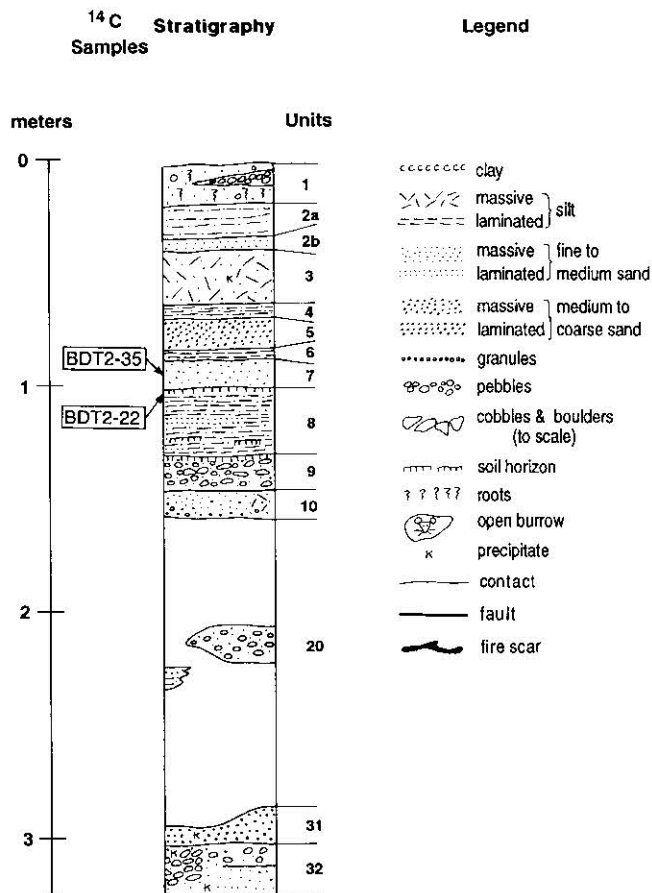

Figure 6. Generalized stratigraphic column of sedimentary deposits in trench 2. Distinctive or laterally extensive units and groups of units are numbered to facilitate discussion. The units consist primarily of debris flow deposits, fluvial deposits, and bioturbated layers. Sedimentary characteristics are represented by symbols shown in the legend.
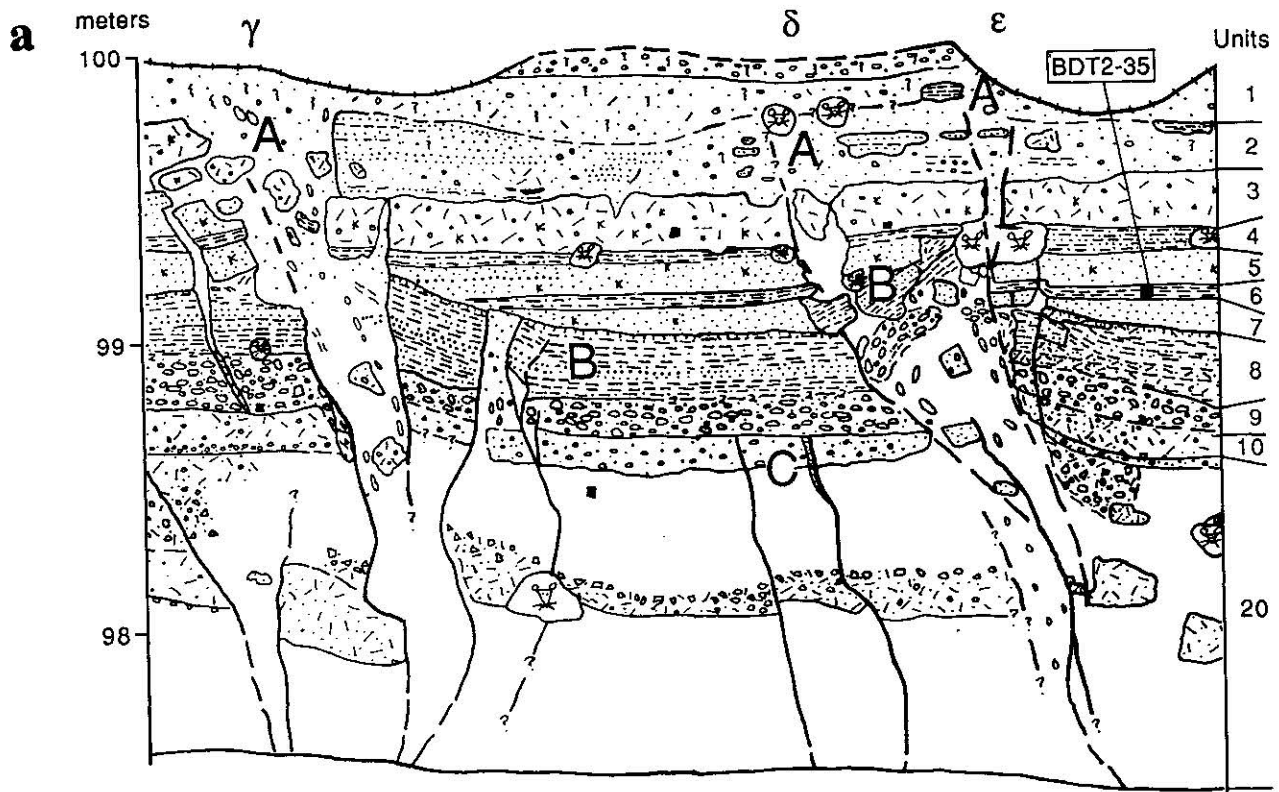
Figure 7. Portions of the walls of trench 2 that display evidence for earthquake disruption A (1857), B, and C. Greek letters indicate fault zones referred to in text. Letters A, B, and C mark the approximate locations of stratigraphic evidence for these events. View is toward the northwest. See Figure 5 for locations and Figure 6 for symbol legend. Blank areas are fault-zone breccia or bioturbated zones.

The upper 1–4 cm of unit 8 is a well-developed, continuous paleosol with root holes of a few millimeters diameter, scattered flakes of carbonized organic matter, and an irregular lower boundary.

Evidence of Earthquakes

Event A: Fort Tejon earthquake. The presence of a 3-m-deep gully only 15 m northwest of trench 2 and disrupted fan topography nearby is a clue that very little sedimentation has occurred at the site of trench 2 since the latest major fault rupture (Figure 3). Indeed, the walls of trench 2 display a 13-m-wide zone of faults, many of which extend upward to the bioturbated surficial units 1 and 2 (Figures 5 and 7). The near-surface fault traces from the most recent rupture are designated "event A." Unit 3, a debris flow bed, is the youngest faulted bed which can be correlated across all major faults in the trench. Although units 2a and 2b display evidence of faulting at the northeastern end of the trench, they are absent in two thirds of the trench on account of bioturbation. In the southwestern half of trench 2, unit 3 is broken by three major faults, labelled α, β, and γ (Figure 5). Beds exhibit facies changes across each of the faults; these changes indicate a strike-slip component of motion. Each fault also has a normal component of motion, northeast side down. Faults δ and ε, at the northeast end of trench 2 also break unit 3 and extend upward into unit 2 on the southeastern wall.

Because the 1857 earthquake generated at least 6.6–6.9 m of slip along the main fault trace at the Phelan fan 3 km

northwest of trench 2 [*Grant and Sieh*, 1993] and 11.0 ± 2.5 m (1σ) of dextral offset across a greater width of the fault zone [*Grant and Donnellan*, 1994], it is very likely that the smaller offset next to trench 2 was formed by surficial rupture in 1857. Therefore the youngest event, A, which breaks units 2 and 3 in the walls of trench 2 is the 1857 Fort Tejon earthquake and its associated foreshocks, aftershocks, and afterslip. In trench 2 the rupture zone of event A (1857) is 13 m wide (Figure 5). The amount of dextral slip can be inferred from the net dextral offset of the nearby stream channel (Figure 3).

Event B: Penultimate earthquake. The youngest deformation event prior to event A occurred when unit 8 was at the surface (Figure 5). At the time of the penultimate earthquake, a thin paleosol had developed on the surface of the laminated silt and sand of unit 8 (Figure 7). The paleosol has a maximum thickness of 5 cm in the northeastern part of the trench. Units 7, 6, and 5 overlie the faulted paleosol surface of unit 8.

Several angular unconformities are clear evidence of deformation between the time of deposition of units 7 and 8 (Figures 5, 7a, and 7c). Just northeast of fault zone γ, on both walls, flat-lying units 6 and 7 pinch out against tilted unit 8. Similarly, unit 7 thins out against upturned unit 8 northeast of fault zone δ-ε on the southeast wall of the trench (Figure 7c). Another angular unconformity exists between faults δ and ε on the southeast wall (Figure 7a). A strand of fault zone α also terminates at the top of unit 8 and is
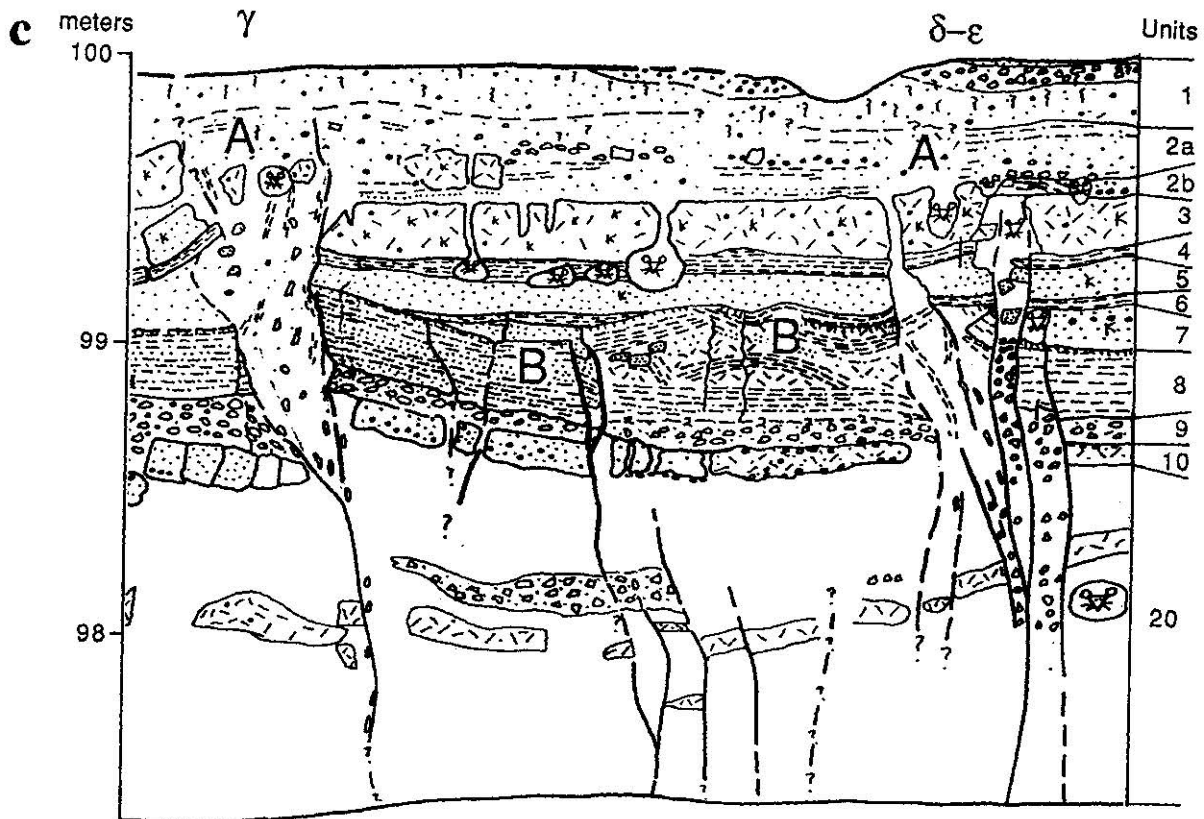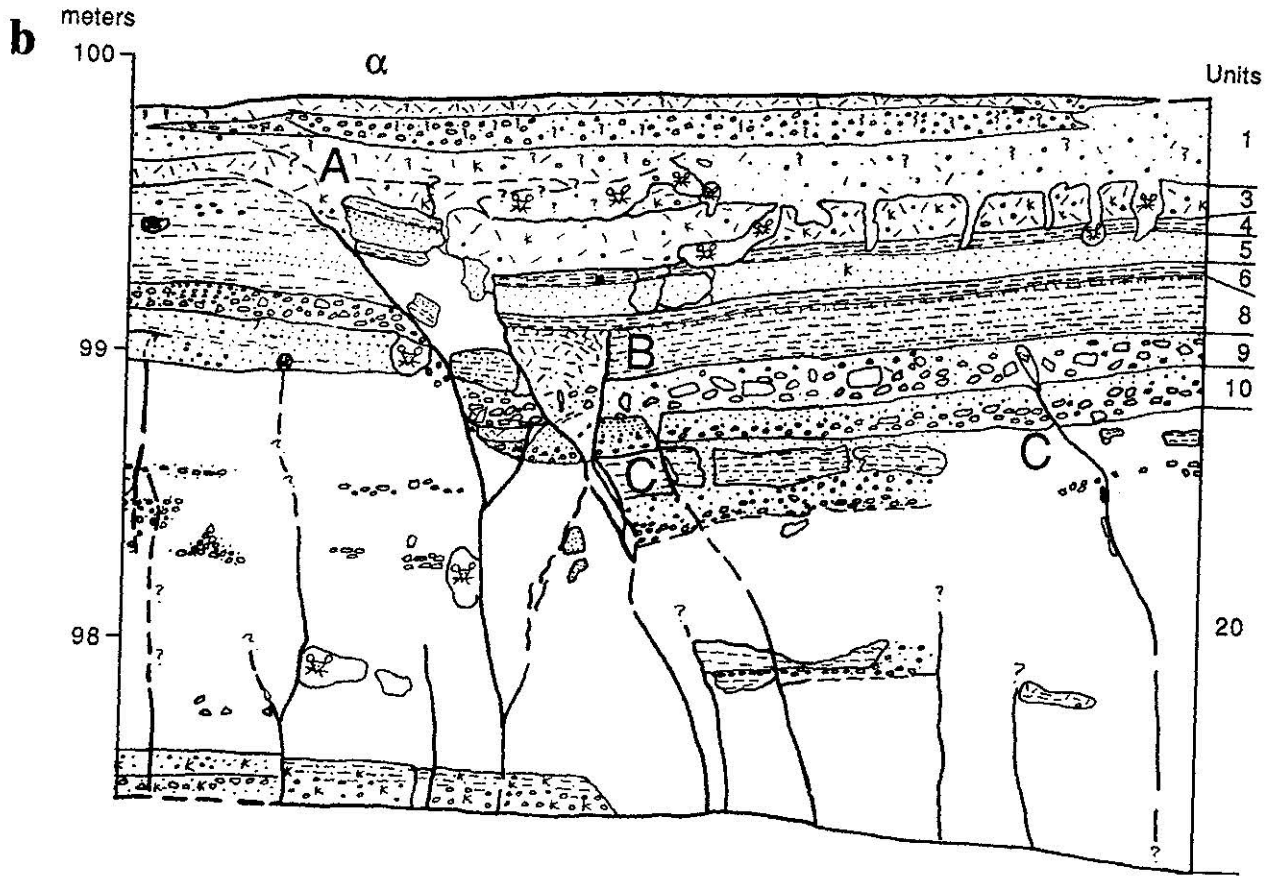
Figure 7.   (continued)

Table 1. Radiocarbon Samples

Sample	$\delta^{13}C$	Radiocarbon Years B.P.	Calendar Years		Description
			1σ	2σ	
BDT2-22	−11.3	445 ± 40	A.D. 1425–1465	A.D. 1405–1510	grass fragments
BDT2-35	−12.0	580 ± 40	A.D. 1310–1405	A.D. 1290–1415	charred twig
BDT3-17	−21.6	2750 ± 70	B.C. 993–828	B.C. 1060–800	charcoal
BDT3-30	−9.4	2545 ± 50	B.C. 800–603	B.C. 812–530	shell, genus Helminthoglypta
BDT3-46	−25[a]	1965 ± 99	A.D. 98–126	B.C. 200–A.D. 250	charred plant (grasses?)
BDT4-39	−25[a]	815 ± 45	A.D. 1180–1263	A.D. 1063–1274	charcoal
BDT4-40	−12.9	995 ± 45	A.D. 998–1035	A.D. 970–1159	charcoal
BDT4-53	−25.9	1720 ± 55	A.D. 241–395	A.D. 144–430	charred woody plant material
BDT4-57	−10.8	595 ± 50	A.D. 1291–1405	A.D. 1280–1430	charred plant material
BDT4-64	−23.7	775 ± 30	A.D. 1235–1269	A.D. 1218–1276	charred plant fragments
BDT4-66	−11.35	940 ± 50	A.D. 1020–1162	A.D. 1000–1220	charcoal
BDT4-76	−10.4	795 ± 58	A.D. 1195–1271	A.D. 1054–1280	charcoal
BDT4-84	−11.0	650 ± 30	A.D. 1283–1379	A.D. 1277–1392	charcoal
BDT4-89	−25[a]	820 ± 80	A.D. 1159–1270	A.D. 1029–1290	charred plant (grass?)

Samples analyzed by the National Science Foundation AMS Facility at the University of Arizona. Sample number BDT2-22 is the 22nd sample collected from Bidart trench 2. Other samples are named similarly.

[a] $\delta^{13}C$ is assumed to be −25 because sample was too small to permit measurement.

overlain by unfaulted unit 6 on both walls of the trench (Figure 7b).

On the northwest wall of trench 2 between faults zones γ and δ, there is an anticlinal fold composed of comminuted upper unit 8 (Figure 7c). The fold appears to rest above a detachment within a laminated sandy component of unit 8. The anticline probably resulted from compression between fault zones γ and δ during event B. A fissure cuts unit 8 on the southwest limb of the anticline. Sands and silts of units 6 and 7 overlie and fill in the fissure. Hence the event occurred when the top of unit 8 was the ground surface. The anticlinal folding of unit 8 suggests that it may have been wet enough during the earthquake to deform semiductily. Opposite the fold on the southeast wall between fault zones γ and δ, a 10-cm-wide zone of fault breccia from event B extends to the surface of unit 8 and is covered by unfaulted units 7 and 6 (Figure 7a).

Fault zones α, β, γ, and δ-ε ruptured in both events A and B. All of the angular unconformities noted above are next to faults that also broke in event A. Fault zone β also shows evidence of movement during both events: The apparent offset of unit 8 is greater than the offset of unit 3 across the fault (Figure 5). The total width of the fault zones exposed in trench 2 is approximately the same for events A and B. This suggests that dextral offsets during event B were similar to those that occurred during event A, that is, several meters.

Event C. In trench 2 event C occurred at the end of a depositional hiatus that could hide evidence of additional events. Numerous fault traces terminate at the top of bioturbated unit 20 and in units 9 and 10. These traces represent at least one ground-rupturing earthquake and possibly several. Because bioturbation has destroyed the original stratigraphy in unit 20, it is difficult to correlate beds and faulting events in the lower half of the trench. There are up to three apparent events with fault terminations in units 9 or 10, at the top of unit 20, and in the middle of unit 20 (Figures 5, 7a, and 7b). However, bioturbation in unit 20 may have obliterated the upper part of some traces and not others, leaving the appearance of two or more separate events. The best evi-

dence in support of a multiple event hypothesis is southwest of fault zone α, on both walls, where at least one fault trace terminates below a remnant, unbroken bed in the central part of unit 20. This suggests that more than one rupture event terminates within the thick bioturbated layer.

Additional evidence that event C is more than one earthquake is between fault zones α and β. There several faults terminate at the top of bioturbated unit 20 on the southeast wall of trench 2 (Figure 5). On the northwest wall two traces from the same set of faults appear to extend upward into units 9 and 10 (Figure 7b). Beds 9 and 10 are broken, but no displacement is apparent on either side of the traces, suggesting that the amount of offset, if any, is small. These upward terminations may have formed during an earthquake which ruptured above unit 20, or the upper part of these traces may be misidentified rodent holes or settling of units deposited above fault traces formed during event C.

Thus at least one and probably several earthquakes ruptured to the surface of unit 20. We define the earthquake as event C and recognize that in trench 2 event C could represent up to three earthquakes which cannot be stratigraphically separated because of bioturbation during a depositional hiatus preceding event C. The width of the fault zone which ruptured during event C is approximately the same as for events A and B and is located slightly further to the southwest.

Radiocarbon Dating of Event B

Numerous fragments of detrital charcoal and organic material were embedded in the walls of all three trenches, but very few of the samples were large enough to be dated with AMS (Table 1). Some of the dated samples from trenches 3 and 4 were too small to measure the $\delta^{13}C$ ratio, which complicates the interpretation of their ages. A more serious complication is the detrital nature of most samples. The radiocarbon age of detrital wood can be considerably greater than the depositional age of a bed which contains it [*Blong and Gillespie*, 1978; *Nelson*, 1992]. In the Carrizo Plain, radiocarbon dates on samples from the same stratum

can differ by several hundred years [*Grant and Sieh*, 1993]. Thus the radiocarbon ages of samples must be evaluated with other information to determine the age of the events.

The date of event B is constrained by analysis of two radiocarbon samples from trench 2. The uppermost part of the paleosol at the surface of unit 8 contained nonwoody flakes of organic material resembling blades of grass which we collected for AMS dating (sample BDT2-22). The flakes appeared to be in situ plant material. The radiocarbon age of sample BDT2-22 yields a 2σ calendric age range of A.D. 1405–1510. The measured δ^{13}C is consistent with values reported elsewhere for C-4 plants [*Smith and Epstein*, 1971]. A detrital, woody sample (BDT2-35) was collected from overlying unit 6. It yields an overlapping but older 2σ calendric age range of A.D. 1290–1415. Since this sample is detrital, it may be older than the bed that contained it. However, the grassy fragments of sample BDT2-22 were preserved in situ, are not detrital, and probably had a short lifespan.

Since the paleosol is broken by event B, the earthquake occurred after the paleosol had formed. Since the paleosol contained in situ flakes of organic material dated A.D. 1405–1510, the earthquake occurred sometime after a date within that range. We suspect that event B occurred within the date range A.D. 1405–1510. Our reasoning is based on evidence from trench 1. As noted earlier, *Prentice and Sieh* [1989, also written communication, 1993] mapped five paleosols in the sediments deposited after the last earthquake. One additional paleosol began forming in 1991. If we assume that the last surface rupture was the 1857 Fort Tejon earthquake, then at least six paleosols have formed since 1857. On average each paleosol represents a time span of about two decades. The radiocarbon age range of sample BDT2-22 spans a time period (A.D. 1405–1510) that is several times longer than the estimated age range of the paleosol that was at the ground surface when event B occurred. Therefore we hypothesize that the date range A.D. 1405–1510 includes the date of event B. Since the paleosol formed over a few decades and the earthquake occurred soon after paleosol formation, the century-long radiocarbon date range of the soil age should contain the date of the earthquake. Therefore we estimate the date of event B to be between A.D. 1405 and 1510.

Trenches 3 and 4 and Older Events

Trenches 3 and 4 were cut next to the larger (14–18 m) offset to find evidence of earthquakes prior to event B. Because the stream channel is offset at least twice as much as the channel near trench 2, we assume that the offset formed during slip in earthquakes A and B, at least. It is a reasonable assumption that incision of the channel occurred prior to offset, that is, prior to event B. We hypothesized that this area was the depositional lobe of the Bidart fan during the time of a depositional hiatus in the sections of trenches 1 and 2. We placed trench 3 next to the offset channel to date earthquakes prior to event B and to try to determine the amount of slip associated with the last few earthquakes. Sediment was deposited in a neighboring graben (Figure 4) during the 1991 storms, suggesting to us that enough sediment might have been deposited in the graben to preserve evidence of postincision earthquakes which occurred after the depositional lobe of the fan migrated south-

east. Therefore we excavated trench 4 across the graben to relate the stratigraphic section of trench 3 to the number of earthquakes which occurred after incision of the offset channel.

Structure and Stratigraphy

The sediments and structures in trenches 3 and 4 reflect the depositional environment and structural evolution of a graben. Trench 3 straddles a topographic high, or moletrack, within the fault zone (Figure 4). Thick beds in the central blocks of trench 3 suggest that they were deposited in a graben and subsequently uplifted. Thicker, down-dropped beds below the topographic graben in trench 4 indicate that the structural depression has persisted over several earthquake cycles.

Major fault zones separate stratigraphically coherent blocks within each trench (Figures 8 and 9). A 4-m-wide shear zone underlies the northeastern flank of the moletrack in trench 3. There are major faults at the edges of the graben in trench 4 and paleograben in trench 3.

We correlated beds across faults and between trenches using stratigraphic position, texture, and appearance. Stratigraphic columns in Figure 10 show correlation of individual beds between trenches 3 and 4 and across major faults within the trenches. None of the beds were correlated with beds in trench 2. Most of the ground surface (unit 10) is bioturbated at trenches 3 and 4, consistent with the dearth of recent sedimentation on the northwestern part of the fan. Units 20–70 in the graben near the top of trench 4 are not found in trench 3. Units 20–70 were probably deposited in the graben of trench 4 after the trench 3 graben was filled in and uplifted.

At the northeastern ends of trenches 3 and 4, outside the graben and paleograben, the uppermost meter of section has an identical sequence of beds. Bioturbated unit 200 and overlying beds 80, 100, and 110 can be traced across all major faults in both trenches. Below bioturbated layer 200 is a thick, cobble gravel (unit 220) capped with a locally preserved laminated silt and fine sand bed. The cobble gravel is thickest in the central part of trenches 3 and 4, indicating that it was deposited in a previous longer graben along the fault.

At the base of the southwesternmost exposures of unit 220 is a laminated coarse sand and granule bed (unit 230) in both trenches. Units 220 and 230 rest on silty clay unit 240 which is well exposed in trench 3 and partially exposed in trench 4.

In the outer blocks of both trenches a sequence of beds below unit 200 was not correlateable between or across the trenches. Beds in blocks I and IV have been offset from each other by multiple earthquakes, making correlation difficult. Additionally, both trenches are at the northwestern edge of the Bidart fan. Prior to incision of the channel which currently forms the boundary between the Bidart fan and a fan to the northwest (Figure 2), sediments from the two fans may have interfingered, complicating correlation of the older sediments.

Evidence of Earthquakes

Event A. The proximity of trenches 3 and 4 to the 14–18-m offset channel led us to expect that little deposition would have occurred there since at least two large slip events ago. We expected only very thin and bioturbated beds above the event A horizon, and we expected 1857 and
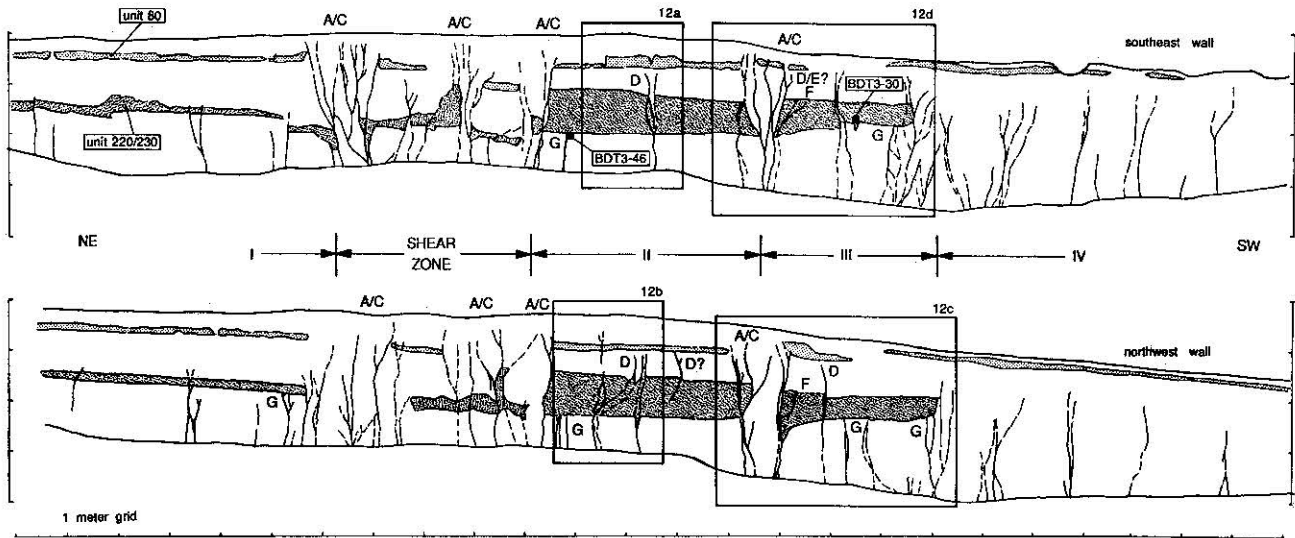
Figure 8. Cross section through sediments in the walls of trench 3 shows fault traces, radiocarbon sample locations, and gravel units 80 and 220/230. The surface of this section shows the profile of a moletrack which formed in association with 14–18 m of dextral slip. At least 2 large-slip events have occurred since the ground surface last received deposition. Thick gravels indicate filling of an older graben produced during earlier slip events. Fault-bounded stratigraphic blocks marked with Roman numerals are discussed in text. Boxes outline stratigraphic areas shown in detail in Figures 12a–12d to accompany discussions of evidence of various disruptions. Clear evidence of earthquakes is marked with capital letters. Selected carbon sample locations are also marked. View is toward the southeast.

event B to be difficult to distinguish in trenches 3 and 4, except in the topographic graben of trench 4. Indeed, numerous fault traces extend to within a few centimeters of the surface in trenches 3 and 4, but the number of earthquakes represented by each of them is difficult to determine outside the graben of trench 4. Recent deposition in the graben, however, has preserved evidence of event A.

Unit 40 ruptured during event A (Figures 11a and 11b)

within the graben. Unit 30 pinches out against fault scarps from event A on the southeast wall and covers faulted unit 40 on the northwest wall of trench 4, which indicates that unit 30 was deposited after the earthquake. The fresh appearance and relatively steep slopes of the graben boundaries suggest that the graben boundary faults also moved during event A (Figure 4).

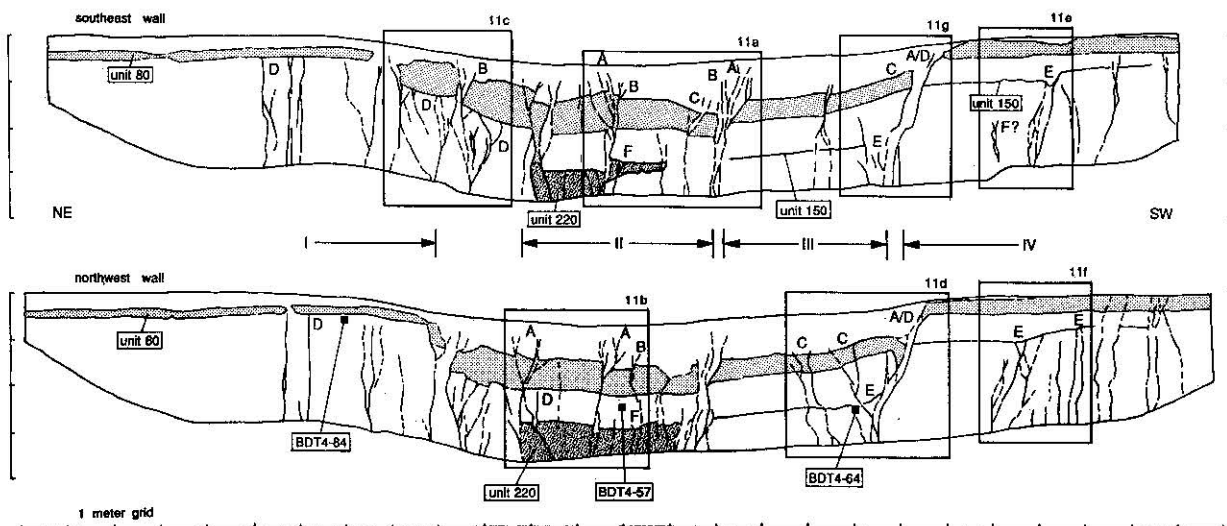The incised stream channel northwest of trench 3 is offset

Figure 9. Cross section through sediments in the walls of trench 4 shows fault traces, radiocarbon sample locations, and units 80, 150, and 220/230. The section shows a tectonic depression, or graben, in which sediments have accumulated. Evidence of several earthquakes is preserved in the sediments. Individual earthquakes are marked with capital letters. Fault-bounded stratigraphic blocks are numbered with Roman numerals keyed to the text. Boxes outline stratigraphic sections shown in detail in Figures 11a–11f. Selected carbon sample locations are marked. View is toward the southeast.
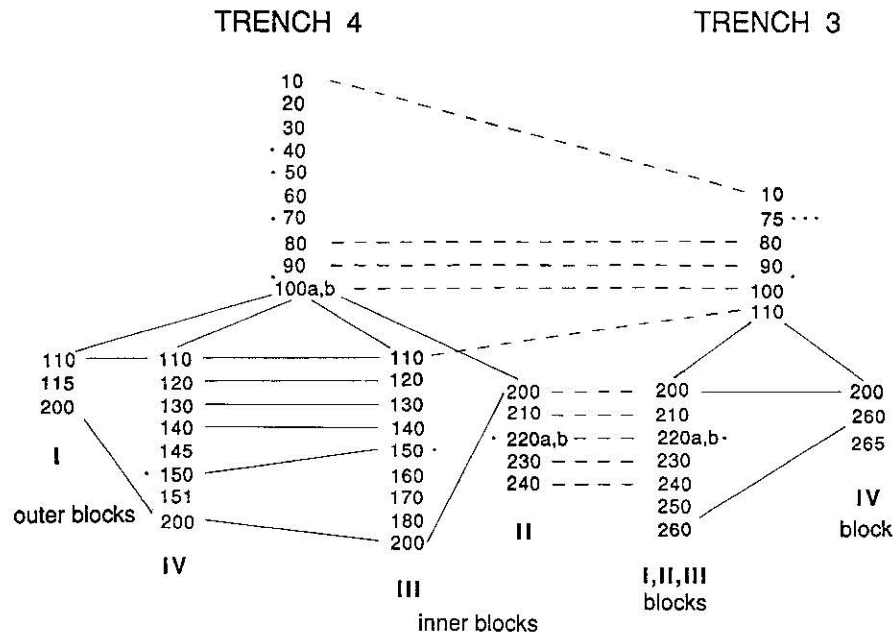
Figure 10. Stratigraphic sequences in trenches 3 and 4. The numbers correspond to units discussed in text and shown in greater detail in Figures 11 and 12. Solid lines join units correlated across faults in each trench. Dashed lines connect units correlated between the trenches. The dots mark earthquake horizons. Stratigraphic blocks are labelled with roman numerals, as in Figures 8 and 9.

14.6–18.4 m (Figure 4). Nearly 7 m of slip occurred on the main trace of the San Andreas during the 1857 earthquake at the Phelan fan, approximately 3 km to the northwest (Figure 1) [*Grant and Sieh*, 1993]. The offset channel at trench 2 indicates that up to 8 m of slip was associated with event A on the Bidart fan. Although slip can vary by several meters over short distances along a fault [*Rubin and McGill*, 1992; *Grant and Donnellan*, 1994], the amount of slip at trench 3 is probably about the same as the slip at trench 2. Therefore event A probably generated approximately half of the channel offset at trench 3.

Event B. Stratigraphic evidence of event B is also preserved in the uppermost beds of the graben in trench 4 and in places can be distinguished from event A. Because most of the fault traces which broke in event B were reactivated in event A and because so little sediment was deposited between the two earthquakes, events A and B are difficult to distinguish from each other except in a few places.

Event B broke beds below unit 40. The best expression of event B is on the northwest wall of trench 4 (Figure 11b), where it is expressed as a single trace that terminates below unit 40. Elsewhere, faults from event B appear to splay outward from fault zones associated with event A (Figures 11a and 11b). These "splays" consistently terminate below unit 40. The existence of major facies changes across fault zones that appear to have moved in both events A and B suggest substantial strike-slip motion (Figure 11a). Substantial facies changes are present across the graben boundary faults as well (Figures 11d and 11c), suggesting that they have been active for more than one event, including event B.

The dearth of sedimentation after deposition of unit 80 in trench 3 prevents determination of the number of earthquakes represented by the near-surface ruptures exposed in the walls of trench 3. The geomorphology of the site,

however, yields indirect evidence for event B. The incised stream channel next to trench 3 is offset approximately twice as much as the channel near trench 2, less than a kilometer away. Thus the larger offset was caused by at least two earthquakes. This is indirect evidence for surficial rupture at trench 3 during event B.

Event C. Event C is distinguishable from events A and B only in the graben sediments of trench 4. It is not separable from A and B in the stratigraphy of trench 3. Where event C ruptured up to the surface of unit 70, faulted unit 70 is covered by undeformed unit 60. This is most pronounced in Figure 11a. There units 70, 80, and 100 are broken and tilted. Several of the fault zones which separate structural blocks with very different stratigraphy may have moved during event C. Unit 60 overlies these beds without disruption. Several minor faults which terminate at the upper surface of unit 70 provide additional examples of event C in trench 4 (Figure 11d). Units 70 and 80 are tilted by faulting during event C. Finally, the main graben boundary fault in Figure 11g displays evidence of event C. Unit 80 is planar bedded but tilted. Overlying unit 70 thins toward the fault, which indicates deposition against a scarp that formed in event C.

There is no direct evidence of event C in trench 3. Presumably, some of the fault traces that ruptured through unit 80 to terminate near the ground surface broke during event C. The dearth of sedimentation after deposition of unit 80 at trench 3 prevents discrimination of individual events younger than unit 80. Surficial unit 10 is bioturbated, and therefore it cannot be correlated with beds in the graben of trench 4 which record events A, B, and C. Because several beds are present (or preserved?) only in the graben in trench 4, they cannot be correlated with the time of channel incision. We can conclude that the stream channel incised after deposition of unit 80. We can even hypothesize that the
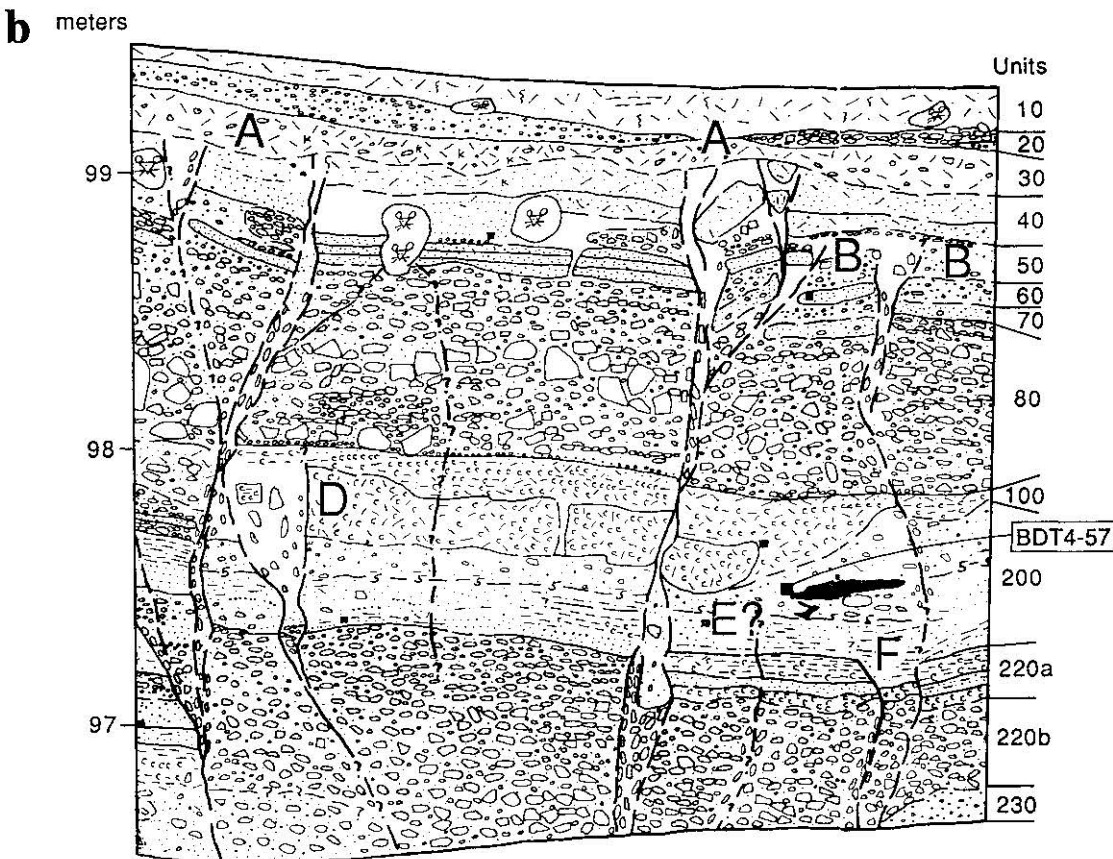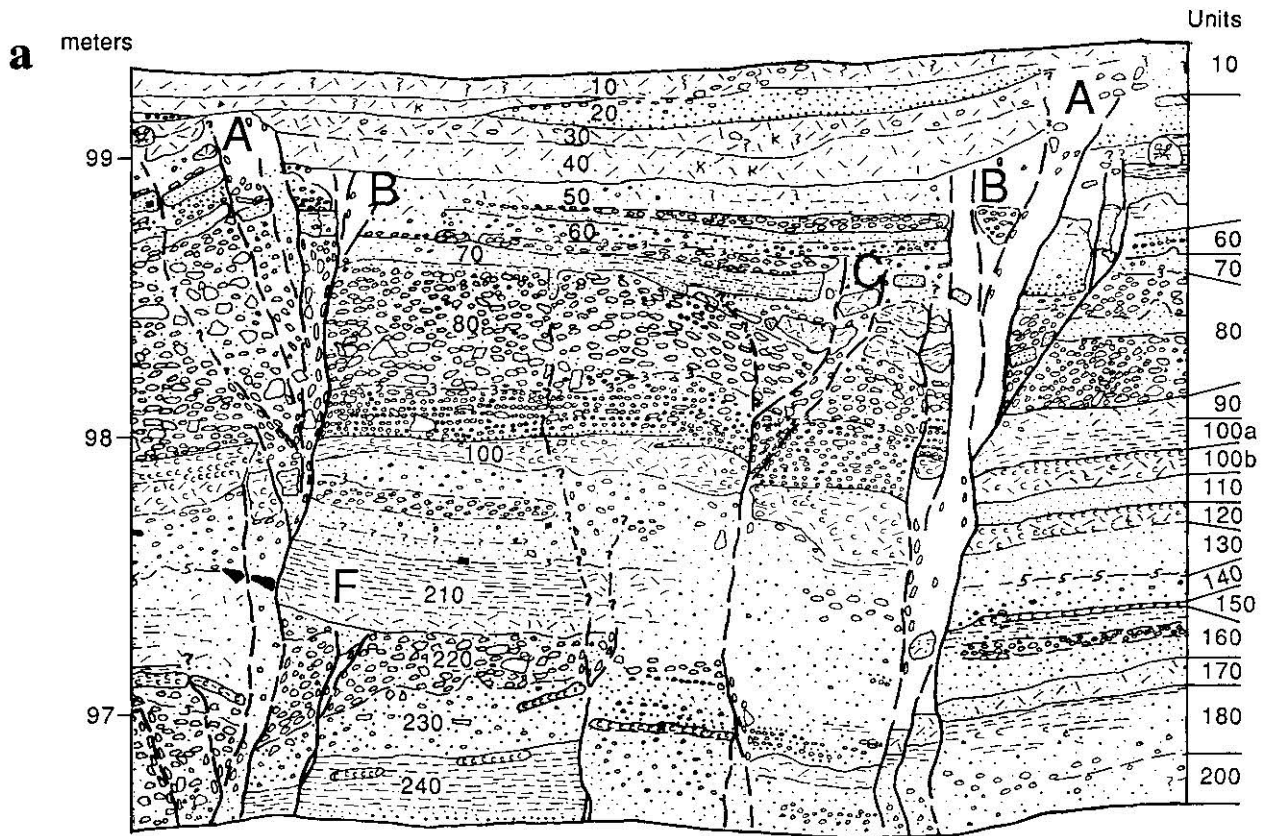
Figure 11. Portions of the southeast (11a, 11c, 11e, and 11g) and northwest (11b, 11d, and 11f) walls of trench 4. Capital letters mark the approximate locations of stratigraphic evidence for the events. Units are numbered. View is toward the southeast. See Figure 9 for locations and Figure 6 for symbol legend. Blank areas are fault-zone breccia or bioturbated zones.
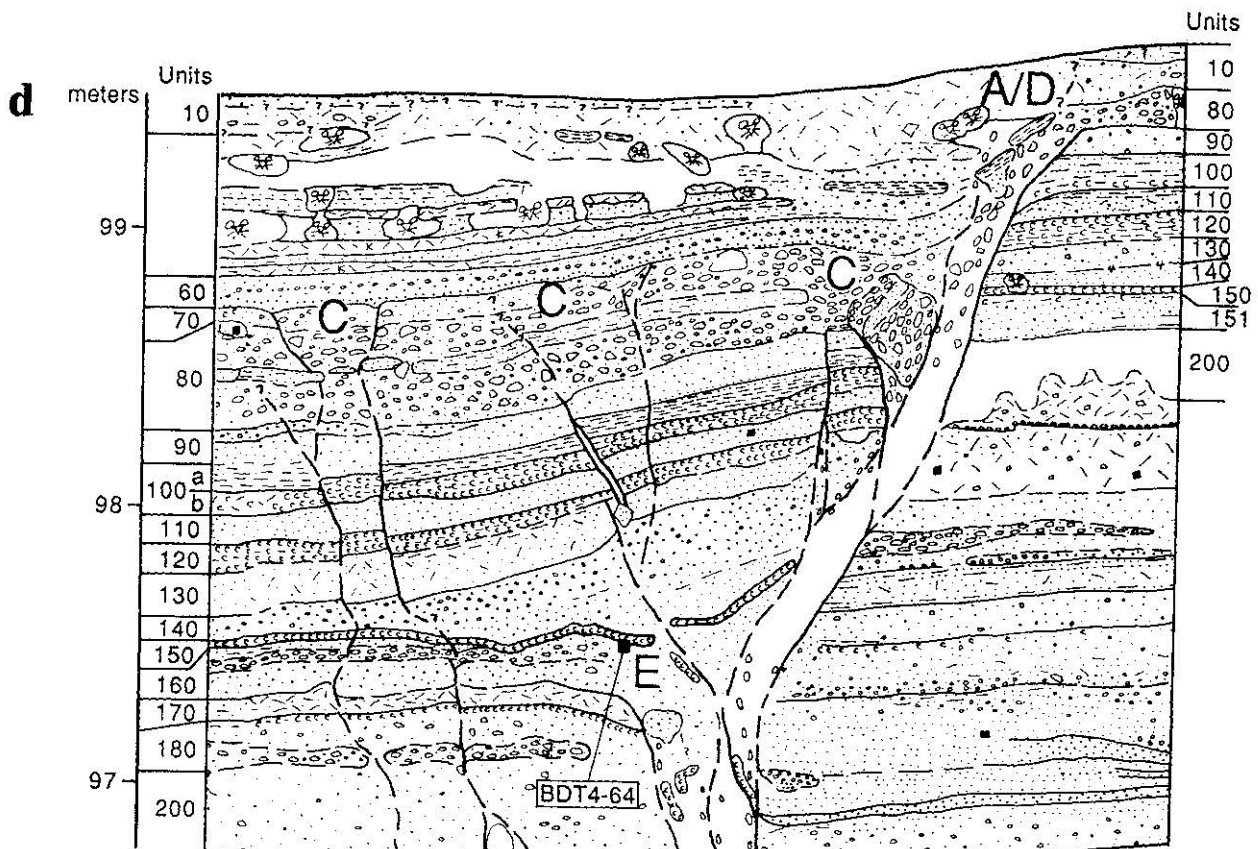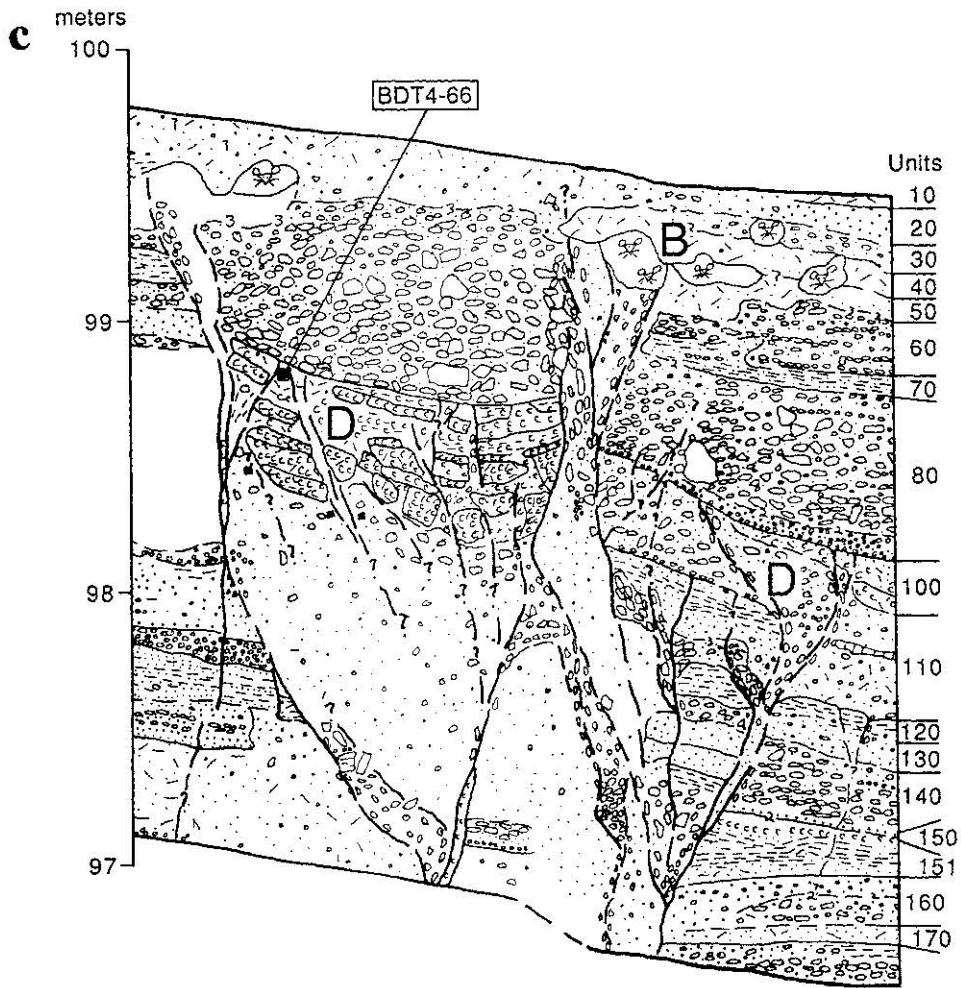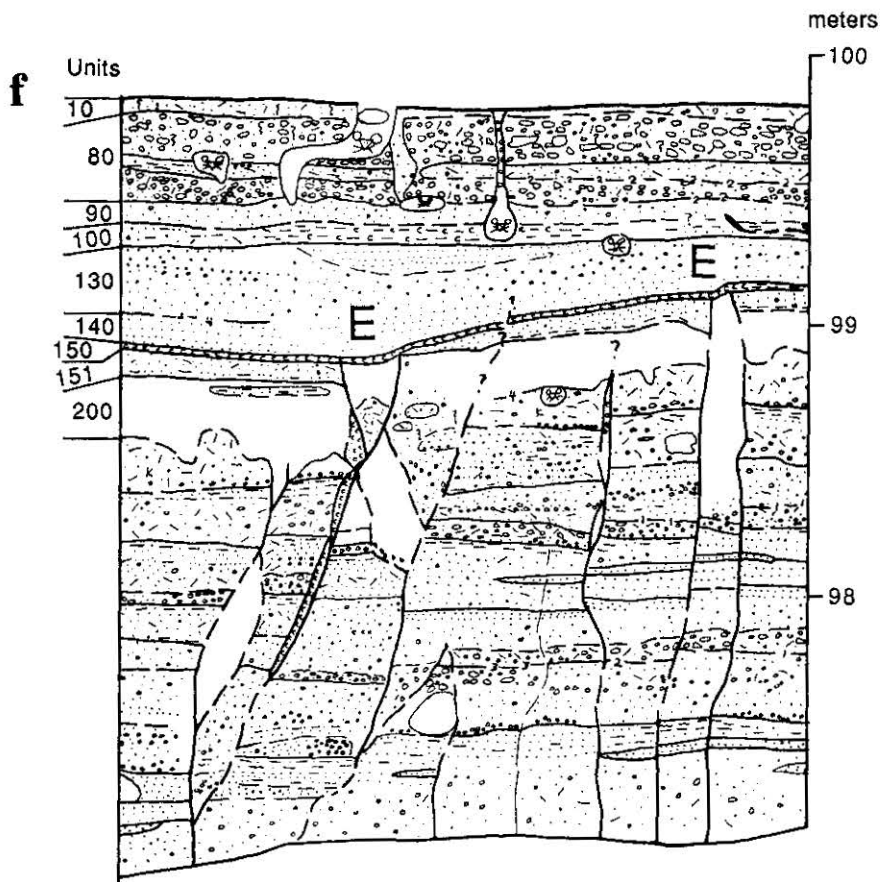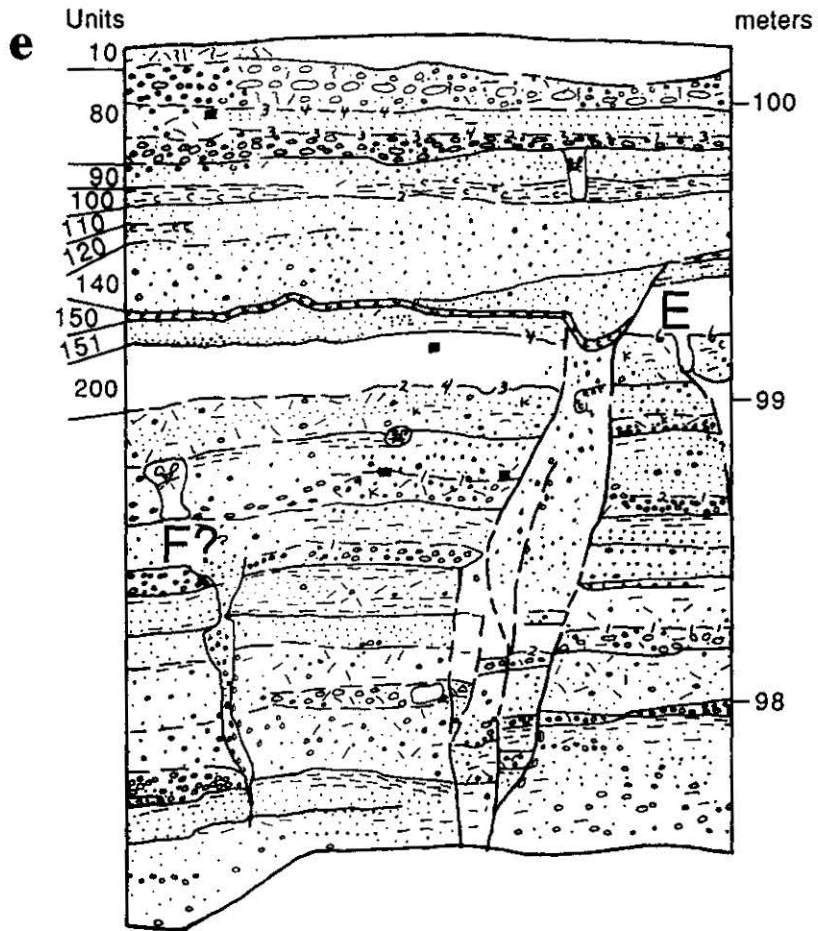
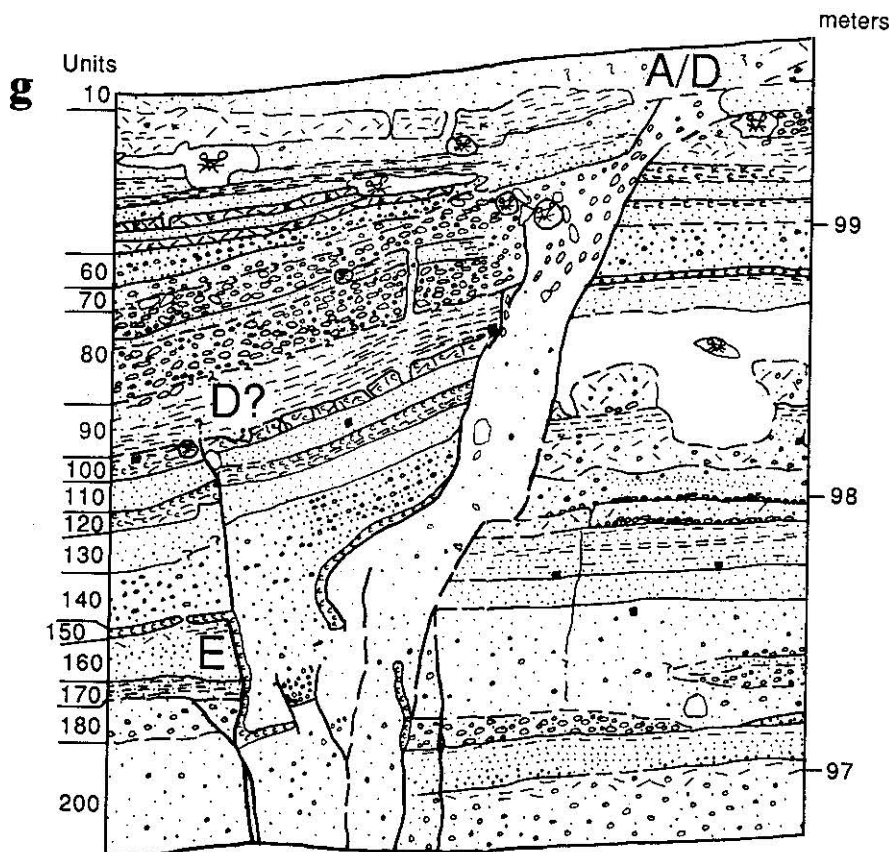Figure 11. (continued)

Figure 11. (continued)

Figure 11. (continued)

channel was incised by the same stormwater which deposited the coarse clasts of unit 80, but this is highly speculative.

Assuming that all large earthquakes younger than unit 80 are recorded and recognized in the graben sediments of trench 4, the channel was offset by a maximum of three events (A, B, and C) and a minimum of two. Thus events B and C jointly, or event B alone offset the channel by 7–11 m.

Event D. Event D breaks unit 100 in trenches 3 and 4. In Figures 12a and 12b from the central part of trench 3 below the crest of the moletrack, fault zones on both walls break unit 100 and appear to terminate in the partially bioturbated layer below the gravels of unit 80. Major faults to the southwest (Figures 12c and 12d) also display evidence of event D on both trench walls. Facies changes and apparent vertical offsets across these faults suggest multiple episodes of slip within the same fault zone. Several traces splaying out from the larger fault zone break unit 100 and terminate below unit 80.

Trench 4 contains abundant examples of event D. On the northwest wall (Figure 11b) a 30-cm-wide shear zone terminates in unit 100, below the sharp base of overlying bouldery gravel of unit 80. On the southeast wall (Figure 11c), unit 100 is extensively disrupted by a 2-m-wide shear zone. The top of the shear zone is the scoured basal contact of unit 80. A similar shear zone is present below unit 80 on the northwest wall, but the upper boundary is not as well defined (Figure 9). Northeast of the graben in block I, several minor faults break unit 100 and the bioturbated zone above it but do not extend upward into the gravels of unit 80 (Figure 9).

Clear evidence of event D is present in the northeast and central parts of trench 4, especially at the northeastern boundary of the graben (Figure 9). In trench 3, unequivocal evidence of event D is only found in the central portion of the graben exposures (in blocks II and III, figure 8). Thus the northeastern graben-boundary fault zone in trench 4 (between blocks I and II) and faults in trench 3 below the crest and southwest flank of the moletrack moved during the same event. They likely formed a continuous fault trace across the graben. The west-northwest striking flank of the moletrack surface (Figure 4) suggests uplift on such a "cross fault." The uplift may have initiated during event D.

Event E. Event E is preserved best in the southwestern half of trench 4, a few centimeters above a bioturbated layer (unit 200). Elsewhere in trench 4 and in all of trench 3 the stratigraphic position of event E would place it within a thick bioturbated layer (unit 200).

In trench 4 a thin clay bed (unit 150) preserves evidence of earthquake E (Figures 11e and 11f). On both walls, several fault traces with measurable offset terminate at unit 150. The clay bed is irregular above the fault terminations. It is not clear whether the bed was at the ground surface at the time of the event or was deposited shortly after the event. In Figure 11f the clay bed is uneven but unbroken at the faults. This suggests that fresh fault scarps may have been draped with a coating of mud after event E. Also, unit 151 appears truncated beneath unit 150. On the opposite wall (Figure 11e) the clay bed appears broken and folded by earthquake E, suggesting that unit 150 was the ground surface at the time of the event. A colluvial wedge shed off the fault scarp buries the clay bed at the fault, indicating that if unit 150 was
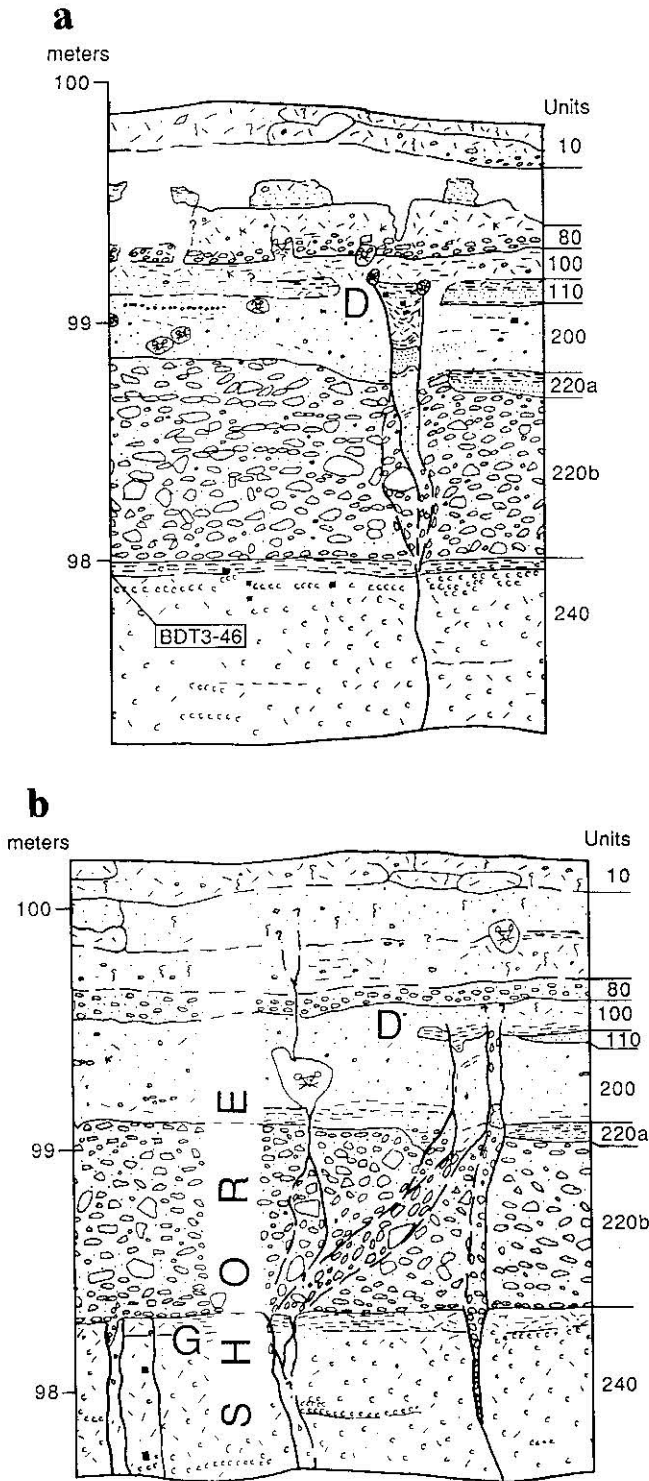
a

b

Figure 12. Portions of the southeast (12a and 12d) and northwest (12b and 12c) walls of trench 3 that display evidence of disruption from earthquakes D through G. Events A (1857), B, and C ruptured to the ground surface after the graben filled with sediment and deposition ceased. Capital letters mark the approximate location of stratigraphic evidence of the earthquakes. Units are numbered. View is toward the southeast. See Figure 8 for locations and Figure 6 for symbol legend. Blank areas are fault-zone breccia or bioturbated zones.

deposited after event E, it was deposited while the scarp was fairly pristine.

Unit 150 is also irregular in the exposure of Figure 11d. The clay bed appears folded near the base of the graben boundary fault, suggesting that it was tectonically deformed or deposited on a concave surface. Faults associated with events A, B, and C have broken and displaced the clay bed at the edge of the graben. This makes it difficult to determine if unit 150 was also broken by event E. On the northwest wall near the base of trench 4 (Figure 11g), however, it appears that a fissure formed during event E or shortly thereafter. The clay bed lines the walls of the fissure. The clay may have fallen into the fissure during event E, or, more probably, the fissure may have been coated by unit 150 clay shortly after its formation. Similar fissures formed during heavy rains a few days after the Borrego Mountain earthquake [*Clark*, 1972]. Similar sedimentary features exposed in trenches at Pallett Creek are interpreted as clay-lined sand-blows which formed during seismically induced liquefaction of fault zone sediments [*Meisling and Sieh*, 1979].

Graben growth during events A–E. In trench 4, events C, D, and E appear to have ruptured alternating flanks of the graben. Clear evidence of event E is limited to the southwestern half of trench 4. The best exposures of event D are in the northeastern half of trench 4 and the central part of trench 3. Uplift of the graben deposits in trench 3 probably initiated with formation of a cross-graben fault between the northeastern part of trench 4 and the central part of trench 3 during event D. The cross fault may have formed in response to uneven deformation and stress distribution across the graben. The alternating pattern may have continued during event C, with slip on faults in the central and southwestern half of the graben in trench 4. The width of the fault zone during event B is uncertain. Deformation occurred across the entire graben at trench 4 during the 1857 earthquake.

Event F. Fault traces from event F break the coarse gravels of unit 220 in both trenches. The best exposures are preserved in trench 3, where the gravels (unit 220b) are capped by a laminated silt and sand bed (unit 220a). On the southeast wall of trench 3 (Figure 12d) the gravels of unit 220b are disrupted by faults which break and offset unit 220a. Unit 210 covers the faulted beds. The fault zone was reactivated during event D and younger event(s). A smaller fault zone to the northeast breaks gravelly unit 220 but does not disrupt unit 210 which was deposited over the fault after event F.

On the northwest wall of trench 3, faults from event F cut through units 220a and 220b (Figure 12c). The faults are overlain by unbroken unit 210, at the margins of two shear zones with evidence of multiple events. Near the southwestern edge of Figure 12c, faults splaying off a wide fault zone cut through the gravel of unit 220 but do not extend to the top of the gravel bed. These traces may be splays of faults which were also active during younger events, or they might be near-surface breaks from event F. At the northeast end of trench 3, in block I, several fault traces break the gravels of unit 220 but do not extend upward into the bioturbated zone above (unit 200, Figure 8). These faults could be either remnants of event E, with the upper part of the traces obliterated by bioturbation, or they could be from event F.

Event F is visible near the base of trench 4. A sand-filled fissure breaking unit 220 (Figure 11a) is interpreted as event F. A fault trace which breaks up through the surface of unit
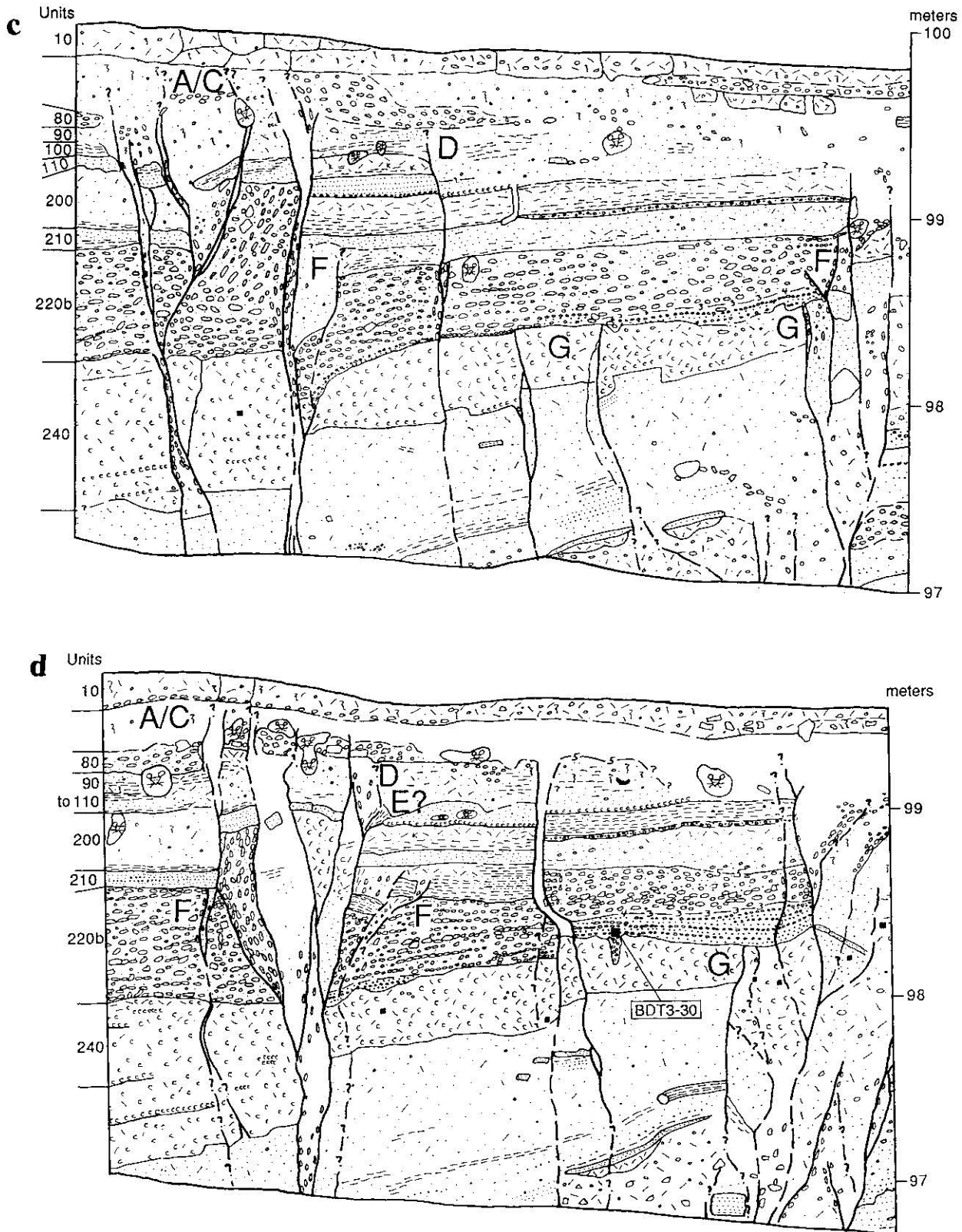
Figure 12. (continued)

220a on the northwestern wall of trench 4 is also attributed to event F.

Event G. Event G breaks a thick, massive, or laminated, silty clay bed (unit 240) near the base of the exposed section.

Since unit 240 is barely exposed at the base of trench 4 (Figure 11a) there are no definitive examples of event G in trench 4. Event G is visible as discrete fault traces a few centimeters wide that terminate at the top of clay-rich unit
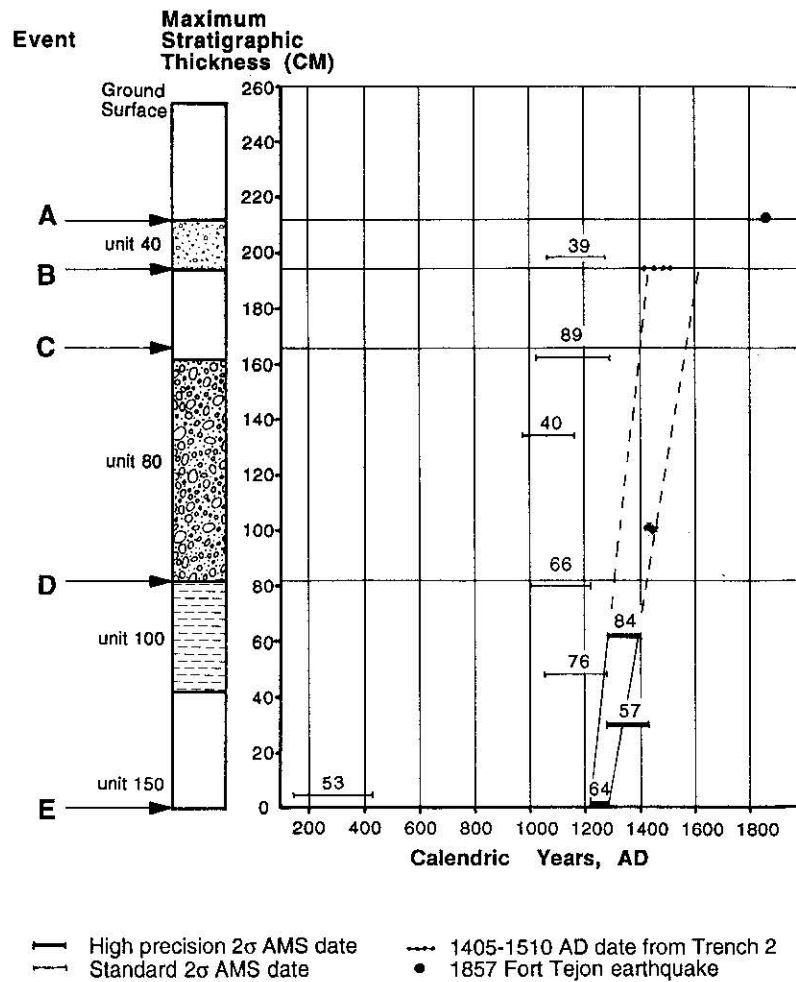
Figure 13. Plot of radiocarbon dates of samples from trench 4. The vertical axis is a generalized stratigraphic column, which uses maximum thicknesses for units above unit 150. Arrows mark the stratigraphic level of events A through E. The horizontal axis is calendric date, A.D. The horizontal bars indicate 2σ calibrated calendric dates of radiocarbon ages of nine samples from trench 4. Sample numbers are above the bars. Sedimentation rate lines drawn through the maximum and minimum dates of samples 64 and 84 also pass through the dates of samples 57 and 76. One of the extrapolated lines (dashed) intersects the age range of event B from trench 2. Thicker bars indicate high-precision dates. Several dates in the upper part of the section are as old or older than the dates near the base of the section, and sample 53 is much older than the others. The apparent stratigraphic age inversion is caused by detrital wood. Detrital contamination prevents determination of the dates of individual events but allows calculation of the average length of intervals between events by using the youngest samples from each stratigraphic level. See Table 1 for analytical details and text for discussion.

240. Fissures at the surface of unit 24 are filled with gravels from overlying unit 220 (Figures 12b and 12c). Differences in the thickness of unit 240 across faults (Figure 12c) and the presence of nearly horizontal slickensides indicate that the discontinuities are faults and not mud cracks.

Radiocarbon Dating of Beds and Earthquakes

Radiocarbon dating of samples from trenches 3 and 4 yields estimates of the dates of events prior to event B. The results of radiocarbon analysis of all dateable samples are summarized in Table 1.

In trench 3, two samples place gross constraints on the date of event G. Sample BDT3-46 was embedded in clay at the top of unit 240, which is faulted by event G. Error bars on the radiocarbon age of this sample are unusually large (Table 1), and the $\delta^{13}C$ was not measureable. We collected a

terrestrial snail shell (sample BDT3-30) from the base of gravel unit 230, which overlies faulted unit 240. The shell is at least 300 years older than the plant material beneath it, making the date of event G difficult to determine. We estimate that event G occurred after deposition of the sample BDT3-46, sometime during or after B.C. 200 to A.D. 250. Event F occurred after event G and prior to event E. In both trenches, bioturbated unit 200 is above the units that are faulted by events F and G. Thus a depositional hiatus occurred after event F and before event E. Therefore we suspect that event F occurred closer in time to event G than to event E.

Dates of younger samples from trench 4 are plotted in Figure 13. From our observations we believe that these samples were collected from intact beds which were not bioturbated. Several samples in the upper part of the section

are as old, or older, than samples near the base of the trench. The lack of appreciable difference in the age of most samples probably is due to their detrital nature. It is possible that a range fire in the Temblor Range, about A.D. 1100, produced charcoal that continued to be carried to the Bidart site for two to three centuries. To minimize dating problems from detrital wood contamination, we assume that the youngest samples represent the closest approximation to the date of a particular stratigraphic level. This allows us to estimate the average length of intervals between events, despite large error bars on the dates of individual events (Table 2).

Average Recurrence Intervals

Radiocarbon dates provide constraints on the time intervals between earthquakes. Sample BDT4-64 (Table 1, Figure 13) was embedded in clayey unit 150, which was either cut by event E or draped the fissure from event E shortly after the earthquake. A high-precision 2σ radiocarbon age for this sample is A.D. 1218–1276. The texture of the sample and its isotopic composition indicate that it is detrital wood. Thus, although it is younger than several samples above it, it may still be older than bed 150, in which it was entombed. Since unit 150 was deposited shortly before or after event E, the earthquake most likely occurred between A.D. 1218 and 1276, or later. Thus five surface ruptures (and four intervals) occurred between A.D. 1218 and 1857.

Sample BDT4-84, of calendar age A.D. 1277–1392 (Table 1, Figure 13), was collected from unit 100 which is faulted by event D. Four earthquakes (and three intervals) have occurred since deposition of the bed containing this sample. The same four earthquakes occurred after deposition of sample BDT4-57, of calendar age A.D. 1280–1430.

If event E occurred in 1218, then the average recurrence interval of events A through E is about 160 years. Uniform recurrence is very unlikely because event B most likely occurred during the period A.D. 1405–1510, 350–450 years prior to 1857. Therefore earthquakes E, D, C, and B must have occurred in relatively rapid succession. The average recurrence interval for these earthquakes can be calculated several ways (Figure 14). If event E occurred in 1218 A.D. and event B in 1510 (the maximum time interval), then the maximum average time between events B, C, D, and E was 97 years. If event B occurred in 1510 and event D in 1277 (the earliest date permitted by samples BDT4-57 and BDT4-84), the average intervals between B, C, and D would be 116 years, but then only 59 years would separate events D and E.

Analysis of stratigraphic data can be combined with the radiocarbon dates to estimate the length of the earthquake intervals. The sedimentation rate can be used, with caveats, as a rough indicator of the time between earthquakes B, C,
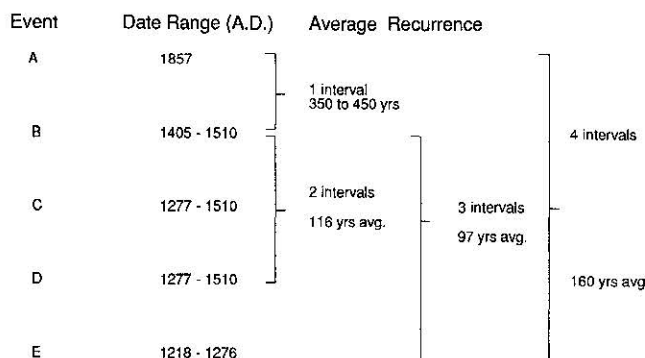
Table 2. Summary of Event Dates

Event	Dates A.D.
A	1857
B	1405–1510
C	1277–1510
D	1277–1510
E	1218–1276
F	after 200 B.C.
G	after 200 B.C.

Figure 14. Visual representation of average recurrence intervals, assuming evenly spaced events. The average recurrence interval has been 160 years, between 1218 and 1857, but ^{14}C dates provide other constraints that show the actual intervals have varied markedly. The interval between 1857 and its predecessor was 350–450 years, whereas the average of earlier intervals is closer to 100 years.

D, and E. The sedimentation rate at a given site on the Bidart fan is episodic because the active depositional lobe of the fan shifts across the fan surface. At a given site the rate of deposition may be semiregular during the time interval when that site is on the active lobe of the fan. As discussed earlier, the site of trench 2 was part of the active fan for a period of time between events A and B. In trench 2, five or six beds (units 2–7) were deposited between events B and A (Figure 7a). However, the incision of the stream channel next to trench 2 occurred prior to its offset in 1857 (event A). Therefore significant deposition must have ceased at the site of trench 2 sometime after event B but prior to event A. Therefore units 2–7 do not represent the entire time interval between events A and B. In trench 4, however, the sedimentation rate can be used to estimate the relative length of time between events C, D, and E because the geomorphology and stratigraphy suggest that the site of trench 4 was on the active fan during these earthquakes. Two thin beds were deposited between events B and C, and at least two thicker beds separate events C and D. There are at least nine beds between events D and E. If the number of beds is even roughly proportional to time, then the time between earthquakes D and E is two to three times as long as the intervals between C and D (and possibly C and B). Thus if we assume that event B occurred in A.D. 1510 and event E in A.D. 1218, the most conservative interpretation yields an interval of 73 years between events B, C, and D and 146 years between events D and E.

Ambiguities in earthquake dates result from the poor quality of our radiocarbon constraints. We hope that more definitive dates can be determined by better dating of strata in the future. The principle contribution of this study is the dating of event B to within the 15th century and the documentation of an apparent cluster of events between the 13th and 15th centuries.

Correlation of Earthquakes

We can use radiocarbon dates of prehistoric earthquakes and accounts of historic earthquakes to hypothesize the length of past rupture events on the southern half of the San Andreas fault (Figure 15). Overlapping error bars on the
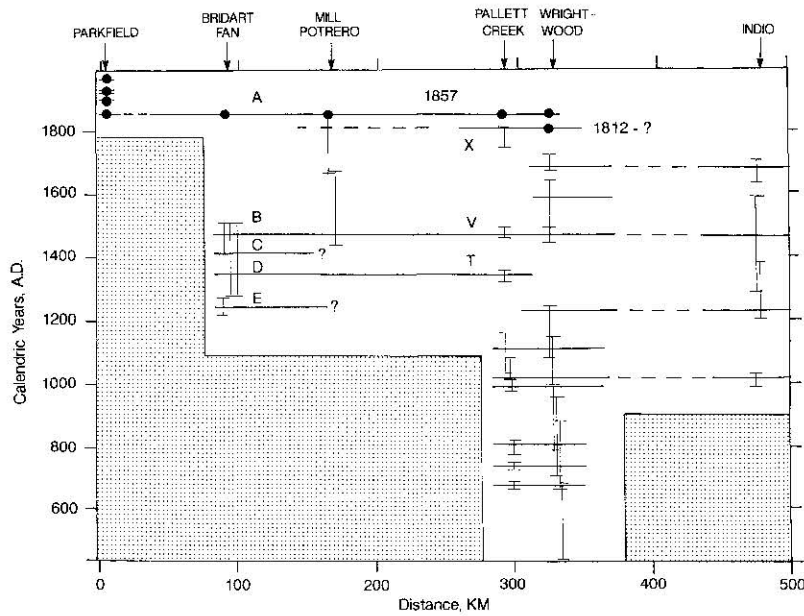
Figure 15. Hypothetical correlation of rupture events along the southern half of the San Andreas fault. Vertical bars are published 95% likelihood errors for dates of earthquakes at paleoseismic sites along the fault. Historical earthquakes are marked with bold dots. Horizontal lines are hypothesized rupture extents of past earthquakes. All lines are conjectural. Dashed lines show a greater degree of uncertainty, for prehistoric and historical events. Bidart fan earthquakes are labelled with capital letters A–E. Events X, V, and T are preserved at Pallett Creek. Paleoseismic dates from Wrightwood are from *Fumal et al.* [1993] and *Weldon* [1991]. Other earthquakes are from summaries of published data by the *WGCEP* [1988]. Length of the 1812 rupture is interpreted from data of *Jacoby et al.* [1988], *Weldon* [1991], and *Fumal et al.* [1993]. Stipple marks areas of no data.

dates of paleoseismic events at different locations allows the possibility of simultaneous rupture during a large earthquake. This method of correlating earthquakes is biased toward hypothesizing larger events, because several smaller ruptures at different sites occurring within a few decades of each other are indistinguishable from a single large earthquake rupturing the same sites. Nonetheless, the potential for great earthquakes on the San Andreas fault was demonstrated by the 1857 and 1906 events, and hypothetical correlation of past events with radiocarbon dates is presently the only way to detect similar large prehistoric earthquakes. With this caveat we estimate the rupture lengths of past Carrizo earthquakes. Our hypotheses may be tested in the future, when more data become available.

The rupture length of the historic 1857 earthquake (event A) has been discussed by *Sieh* [1978] and *Sieh et al.* [1989]. Although there is debate about the northernmost extent of the 1812 rupture [*Jacoby et al.*, 1988, also unpublished data, 1988; *Weldon*, 1991; *Fumal et al.*, 1993], evidence from tree rings near Mill Portrero [*Meisling and Sieh*, 1980] and evidence presented in this paper indicate that it did not reach the Carrizo Plain. The San Andreas fault did not generate a large earthquake in the Carrizo Plain for nearly four centuries prior to the 1857 earthquake.

At all paleoseismic sites along the southern San Andreas there is evidence of an event that could correlate with event B (A.D. 1405–1510) in the Carrizo Plain (Figure 15). At the Pallett Creek and Wrightwood sites an event occurred in A.D. 1480 ± 15 and 1470 ± 20, respectively [*Sieh et al.*, 1989; *Fumal et al.*, 1993]. At Indio an earthquake occurred sometime during the period A.D. 1450 ± 150 [*Sieh*, 1986].

Recent studies indicate that the penultimate Indio event probably occurred in the 15th century (T. Rockwell, personal communication, 1993). Thus the event-B rupture may have been as long or longer than that of the 1857 earthquake. Alternatively, several shorter ruptures may have generated earthquakes along the southern half of the fault in rapid succession within a few decades of A.D. 1480. At this time the error bars on radiocarbon dates of event B are too large to test the hypothesis of simultaneous rupture.

Contrary to hypotheses of infrequent, large magnitude Carrizo earthquakes, closely spaced events in the Carrizo Plain may have been produced by both short and long ruptures of the San Andreas fault. Only two of the last three prehistoric Carrizo events (B and either C or D) can correlate with earthquakes recorded at Pallett Creek to form a large earthquake similar to the 1857 event. We propose that event D was the same earthquake as event T (1329–1363) at Pallett Creek [*Sieh et al.*, 1989] and was probably similar to the 1857 earthquake in size and rupture extent. Our reasoning is based on the radiocarbon date of event D and additional stratigraphic information that suggests the time interval between D and E was twice the time interval between B and C or C and D. If we assume that event E occurred in A.D. 1218 and B in A.D. 1480, then stratigraphic data suggest dates near ~A.D. 1349 and 1415 for events D and C, respectively. The estimated date of event D falls within the 2σ calendar date range of event T (1329–1363). Even without stratigraphic data the error bars on radiocarbon dates of Carrizo event D are large enough to permit simultaneity of events D and T.

If event B is the A.D. 1480 ± 15 earthquake at Pallett

Creek, then event C does not appear to correlate with earthquakes at either Pallett Creek or Wrightwood (Figure 15). Thus either event C is missing from the earthquake record at Pallett Creek, which is unlikely because the Pallett Creek record is nearly continuous between ~A.D. 1400–1812, or event C involved a more northerly section of the fault. Similarly, event E ruptured the San Andreas in the Carrizo Plain but is not found in the earthquake record at Pallett Creek. Thus events C and E might have been smaller than A, B, and D, (see Figure 15) although all the events reported herein were large enough to generate substantial surficial rupture in the Carrizo Plain.

A plausible alternative interpretation is that event C correlates with the A.D. 1480 ± 15 earthquake at Pallett Creek. If that is the case, then events B and E would have been "Carrizo earthquakes" whereas events A, C, and D could have been larger southcentral San Andreas earthquakes. Such a hypothesis would require extreme clustering, because if event C occurred in A.D. 1480 ± 15, only a few decades could have separated events B and C.

A large earthquake may have ruptured the southern San Andreas fault between Wrightwood and Indio within a few decades of either event D or E, perhaps in a pattern of alternating rupture similar to the sequence of 1857 and 1906 earthquakes in southcentral and northern California, respectively. Prior to event E, the Bidart paleoseismic record is poor. A depositional hiatus at the sites of Bidart fan trenches 3 and 4 may not have preserved evidence of additional large earthquakes between events F and E.

Discussion

Despite uncertainties in the earthquake dates and their lengths of rupture, the data we have presented offer new insight into the behavior of the San Andreas fault. Dates of earthquakes at the Bidart fan demonstrate that the San Andreas fault in the Carrizo Plain does not always produce nearly periodic, large earthquakes separated by unusually long recurrence intervals, as originally proposed by Sieh and Jahns [1984]. This is an important observation because many models of fault behavior [Sykes and Seeber, 1985; Stuart, 1986; Sykes and Nishenko, 1984; Rundle, 1988; Sieh et al., 1989; WGCEP, 1988; Ward, 1992] relied heavily upon this characterization of the so-called Carrizo segment of the San Andreas fault.

Our findings are contrary to this characterization. We find that during the past eight centuries, the fault has been characterized by a 200–300-year cluster of large earthquakes, followed by 400 years of quiescence, followed in turn by the great 1857 earthquake. This irregular pattern is similar to the temporal clustering first reported for the San Andreas fault at Pallett Creek [Sieh et al., 1989], where a 1500-year-long record consists of four century-long clusters of two or three large events each, punctuated by three periods of dormancy, each two to three centuries long.

Although temporal clusters of earthquakes have been reported within certain regions [Einarsson et al., 1981; McGuire and Barnhard, 1981; Thatcher, 1989], and along some other fault zones [Ambrayseys, 1970; Ando, 1975] historical patterns of temporal clusters have not been widely recognized. Historical examples are limited to short overlaps between adjacent regions (for example, the few-kilometer overlap between adjacent ruptures of the North Anatolian fault in 1939 and 1942).

We speculate that incomplete strain release during large earthquakes may allow temporal clustering at the Bidart fan and Pallett Creek sites. Heaton [1990] proposed that rupture occurs as a self-healing slip pulse that propagates so quickly along the fault that release of all the accumulated strain may be incomplete. This phenomenon could lead to multiple, clustered failures of the fault near the end of an interseismic cycle. The period between the end of one temporal cluster and the end of the next might best be termed a "supercycle" because the cycle terminates in several events rather than just a single large earthquake.

If the temporal clustering that we describe has a deterministic cause, then it is interesting to ask if we are currently within a cluster. The time since the last earthquake in the Carrizo Plain is approximately the same as the maximum calculated recurrence time within the cluster of events B, C, D, and E but much less than the 350–450 years between event B and the 1857 earthquake. Is the Carrizo Plain currently within an earthquake cluster and therefore likely to rupture again soon, perhaps triggered by a Parkfield earthquake? Or is it between earthquake clusters in midcycle with a low probability of an event, as predicted by the WGCEP [1988]?

Our results challenge the concept that the "Carrizo segment" of the San Andreas fault possesses an unusually high strength. This concept arose from geomorphic observations suggesting that offsets of 9–15 m each have accompanied the past several earthquakes there [Sieh and Jahns, 1984]. Although we have confirmed the large offset they attributed to the 1857 earthquake [Grant and Sieh, 1993; Grant and Donnellan, 1994], similarly large or even larger offsets may not have occurred during the earlier earthquakes. In fact, the tight temporal clustering of four large events in the 13th, 14th, and 15th centuries seriously jeopardizes the validity of one of Sieh and Jahns' assumptions: that new gullies have been cut across the fault more frequently than large earthquakes have occurred. The width of the fault zone and the height of scarps formed during each of these events is similar to that of the 1857 event, so we can be reasonably certain that the amount of offset in each of these events was at least a meter. Beyond this, however, we are hard-pressed to constrain the size of the offsets for these four events. All we know is that 7–11 m of dextral slip resulted from either events B and C combined or from event B alone. Resolution of this issue must await further excavations.

If the strength or frictional resistance of a fault segment is proportional to its average period of recurrence, then the Carrizo segment is not much stronger than the Mojave segment. The longest interval in the Carrizo Plain in this millenium is about 400 years (15th century to 1857). The longest interval at Pallett Creek, along the Mojave segment, is not much shorter: about 350 years (approximately 1480–1812). The average recurrence interval for the Carrizo and Mojave segments are about 160 and 130 years, respectively. Thus if recurrence interval is proportional to strength, as assumed by Rundle [1988] and Ward [1992], and if our record is long enough to estimate the longer-term average recurrence interval, then the San Andreas fault in the Carrizo Plain is only about 20% stronger than at Pallett Creek.

Our data are also pertinent to discussions about segmentation of the San Andreas fault and the characteristic-earthquake model. Proponents of the characteristic-earthquake model [Schwartz and Coppersmith, 1984]

hypothesize the existence of a Carrizo segment of the San Andreas fault [*Rundle*, 1988; *Sykes and Nishenko*, 1984; *Stuart*, 1986] that breaks only in great earthquakes several centuries apart. Later models have delineated a Carrizo segment based on *Sieh and Jahns'* [1984] estimates of the amount of slip in previous earthquakes [*Sieh et al.*, 1989; *WGCEP*, 1988]. But unlike the Wasatch fault zone, which can be divided into segments on the basis of fault discontinuities and dates of prehistoric earthquakes [*Schwartz and Coppersmith*, 1984], no obvious geometric features aid in determination of boundaries for the hypothesized Cholame, Carrizo, and Mojave segments of the San Andreas fault. Whereas the central creeping segment of the San Andreas fault is easily defined by historical behavioral contrasts with adjacent locked segments, and a segment boundary in the vicinity of San Gorgonio Pass may be defended on the basis of unusual structural complexity, the Cholame, Carrizo, and Mojave segments form one nearly continuous trace. There are no stepovers along this reach wider than the 5-km theoretical and observational upper limit for propagation of ruptures along strike-slip fault zones [*Harris and Day*, 1993].

In the absence of discrete structural boundaries, the variation in slip along the 1857 rupture and estimates of slip in previous events have been used to estimate the length and properties of these segments. In 1857 the amount of slip along portions of the Carrizo segment was as great as 9–10 m, whereas it was several meters lower along the adjoining Cholame and Mojave segments and in places along the Carrizo segment [*Sieh*, 1978; *Salyards et al.*, 1992; *Grant and Sieh*, 1993]. However, the ambiguities we have noted for the slip associated with previous earthquakes at the Bidart site raise doubts about how characteristic the 1857 value is. Thus the use of differences in slip magnitude to delineate segments is tenuous at this time.

Currently, the most reliable basis for retaining the concept of segmentation along the southern half of the San Andreas fault is the different earthquake histories available from the Bidart fan, Pallett Creek, and Wrightwood sites [*Sieh et al.*, 1989; *Fumal et al.*, 1993]. Figure 15 shows that dates of prehistoric earthquakes at Bidart fan are markedly different than those at Pallett Creek. Likewise, there are significant differences in the records of earthquakes at the Pallett Creek and Wrightwood sites. By this criterion, Carrizo, Mojave, and San Bernardino segments exist, but their boundaries are poorly constrained.

The data from the Bidart fan site are meager, but they do allow us to place incrementally greater constraints on the behavior of the San Andreas fault. Earthquake forecasts and probability calculations may be improved by incorporating models of irregular earthquake occurrence. A clustered earthquake model is but one conceptual model that describes the small set of paleoseismic data for the San Andreas fault. Nonetheless, it is an improvement over theoretical models of regular earthquake recurrence proposed for the Carrizo Plain [*Sieh et al.*, 1989]. As more dates become available, our ability to discern patterns of past earthquakes will improve. Eventually, we hope that a relatively complete paleoseismic data set will allow forecasting of future earthquakes.

References

Ambrayseys, N., Some characteristic features of the Anatolian fault zone, *Tectonophysics*, *9*, 143–165, 1970.

Ando, M., Source mechanisms and tectonic significance of historic earthquakes along the Nankai trough, Japan, *Tectonophysics*, *27*, 119–140, 1975.

Blong, R. J., and R. Gillespie, Fluvially transported charcoal gives erroneous ^{14}C ages for recent deposits, *Nature*, *271*, 739–741, 1978.

Bonilla, M. G., and J. J. Lienkaemper, Visibility of fault strands in exploratory trenches and timing of rupture events, *Geology*, *18*, 153–156, 1990.

Clark, M., Surface rupture along the Coyote Creek fault, in *The Borrego Mountain Earthquake of April 9, 1968. U.S. Geol. Surv. Prof. Pap.*, *787*, 55–86, 1972.

Einarsson, P., S. Bjornsson, G. Foulger, R. Stefansson, and T. Skaftadottir, Seismicity pattern in the south Icelan seismic zone, in *Earthquake Prediction: An International Review, Maurice Ewing Ser.*, vol. 4, edited by D. W. Simpson and P. G. Richards, pp. 141–152, AGU, Washington, D. C., 1981.

Fumal, T. E., S. K. Pezzopane, R. J. Weldon II, and D. P. Schwartz, A 100-year average recurrence interval for the San Andreas fault at Wrightwood, California, *Science*, *259*, 199–203, 1993.

Grant, L. B., and A. Donnellan, 1855 and 1991 surveys of the San Andreas fault: Implications for fault mechanics, *Bull. Seismol. Soc. Am.*, in press, 1994.

Grant, L. B., and K. Sieh, Stratigraphic evidence for seven meters of dextral slip on the San Andreas fault during the 1857 earthquake in the Carrizo Plain, *Bull. Seismol. Soc. Am.*, *83*, 619–635, 1993.

Harris, R. A., and S. M. Day, Dynamics of fault interaction: Parallel strike-slip faults, *J. Geophys. Res.*, *98*, 4461–4472, 1993.

Heaton, T. H., Evidence for and implications of self-healing pulses of slip in earthquake rupture, *Phys. Earth Planet. Inter.*, *64*, 1–20, 1990.

Huang, J., and D. L. Turcotte, Evidence for chaotic fault interactions in the seismicity of the San Andreas fault and Nankai trough, *Nature*, *348*, 234–236, 1990.

Jacoby, G., P. Sheppard, and K. Sieh, Irregular recurrence of large earthquakes along the San Andreas fault—Evidence from trees, *Science*, *241*, 196–199, 1988.

King, C., Multi-cycle slip distribution along a laboratory fault, *J. Geophys. Res.*, *96*, 14,377–14,381, 1991.

Matsuda, T., Y. Ota, M. Ando, and N. Yonekura, Fault mechanism and recurrence time of major earthquakes in southern Kanto district, Japan, as deduced from coastal terrace data, *Geol. Soc. Am. Bull.*, *89*, 1610–1618, 1978.

McGuire, R. K., and T. P. Barnhard, Effects of temporal variations in seismicity on seismic hazard, *Bull. Seismol. Soc. Am.*, *71*, 321–334, 1981.

Meisling, K., and K. E. Sieh, Possible emplacement history of a sandblow structure at Pallett Creek, California, in Geological Excursions in the Southern California Area, edited by P. L. Abbott, pp. 63–66, Dept. of Geol. Sci., San Diego State Univ., San Diego, Calif., 1979.

Meisling, K. E., and K. E. Sieh, Disturbance of trees by the 1857 Fort Tejon earthquake, California, *J. Geophys. Res.*, *85*, 3225–3238, 1980.

Nelson, A. R., Discordant ^{14}C ages from buried tidal-marsh soils in the Cascadian subduction zone, southern Oregon coast, *Quat. Res. NY*, *38*, 74–90, 1992.

Prentice, C. S., and K. Sieh, A paleoseismic site along the Carrizo segment of the San Andreas fault, central California, *Eos Trans. AGU*, *70*, 1349, 1989.

Rubin, C. R., and S. F. McGill, The June 28, 1992, Landers earthquake: Slip distribution and variability along a portion of the Emerson fault, *Eos Trans. AGU*, *73*(43), Fall Meeting suppl., 362, 1992.

Rundle, J. B., A physical model for earthquakes, 2, Application to Southern California, *J. Geophys. Res.*, *93*, 6255–6274, 1988.

Salyards, S. L., K. E. Sieh, and J. L. Kirschvink, Paleomagnetic measurement of nonbrittle coseismic deformation across the San Andreas fault at Pallett Creek, southern California, *J. Geophys. Res.*, *97*, 12,457–12,470, 1992.

Scholz, C. H., Earthquakes as chaos, *Nature*, *348*, 197–198, 1990.

Schwartz, D. P., and K. J. Coppersmith, Fault behavior and characteristic earthquakes: Examples from the Wasatch and San Andreas fault zones, *J. Geophys. Res.*, *89*, 5681–5698, 1984.

Sieh, K. E., Slip along the San Andreas fault associated with the great 1857 earthquake, *Bull. Seismol. Soc. Am.*, *68*, 1421–1448, 1978.

Sieh, K. E., Slip rate across the San Andreas fault and prehistoric earthquakes at Indio, California, *Eos Trans. AGU*, *67*, 1200, 1986.

Sieh, K. E., and R. H. Jahns, Holocene activity of the San Andreas fault at Wallace Creek, California, *Geol. Soc. Am. Bull.*, *95*, 883–896, 1984.

Sieh, K. E., M. Stuiver, and D. Brillinger, A more precise chronology of earthquakes produced by the San Andreas fault in Southern California, *J. Geophys. Res.*, *94*, 603–623, 1989.

Sieh, K., et al., Near-field investigation of the Landers Earthquake sequence, April to July 1992, *Science*, *260*, 171–176, 1993.

Smith, B. N., and S. Epstein, Two categories of ^{13}C/^{12}C ratios for higher plants, *Plant Physiol.*, *47*, 380–384, 1971.

Stuart, W. D., Forecast model for large and great earthquakes in Southern California, *J. Geophys. Res.*, *91*, 13,771–13,786, 1986.

Sykes, L. R., and S. P. Nishenko, Probabilities of occurrence of large plate rupturing earthquakes for the San Andreas, San Jacinto, and Imperial faults, California, *J. Geophys. Res.*, *89*, 5905–5927, 1984.

Sykes, L. R., and L. Seeber, Great earthquakes and great asperities, San Andreas fault, southern California, *Geology*, *13*, 835–838, 1985.

Thatcher, W., Earthquake recurrence and risk assessment in circum-Pacific seismic gaps, *Nature*, *341*, 432–434, 1989.

Ward, S. N., An application of synthetic seismicity in earthquake statistics: The middle America trench, *J. Geophys. Res.*, *97*, 6675–6682, 1992.

Weldon, R. J., II, Active tectonic studies in the United States, 1987–1990, U.S. Natl. Rep. Int. Union Geod. Geophys. 1987–1990, *Rev. Geophys.*, *29*, 890–906, 1991.

Working Group on California Earthquake Probabilities (WGCEP), Probabilities of large earthquakes occurring in California on the San Andreas fault, *U.S. Geol. Surv. Open File Rep.*, *88-398*, 1988.

L. B. Grant, Woodward-Clyde Consultants, 2020 E. First Street, Suite 400, Santa Ana, CA 92705. (tel. 714-835-6886, fax 714-667-7147).

K. Sieh, Seismological Laboratory 252-21, California Institute of Technology, Pasadena, CA 91125. (tel. 818-395-6115).